The

ENGINEERS' DIGEST

REVIEW OF ENGINEERING PROGRESS ABROAD

JUN 13 1947

VOL. VIII. No. 5 ENGINEERING LIBRARY MAY, 1947

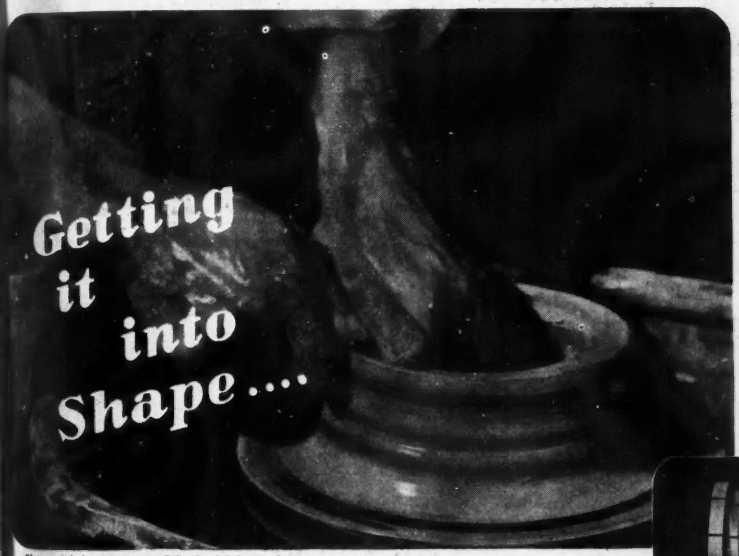

Photograph by courtesy of Salford School of Art.

1. Steering Worm.
2. Acme Thread.
3 & 4. Ball Thread.
5. Special Acme Thread.
6. Valve Seat Inserts.
7. Reduction Gear Tooth Form.
8. "Jet" Propulsion Blade Root.

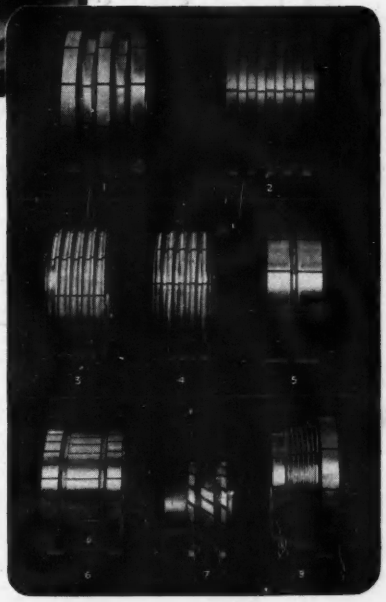

.... is not as easy as it looks. Many years of experience are required before a "technique" can be evolved—and this same experience—40 years to be exact—is responsible for the perfection of Form Grinding on Churchill Precision Machines, using

The "PULCRUSH"

method—the greatest advance yet made in wheel forming. The forms illustrated are a few of the countless contours that can be transferred to the grinding wheel of all machines on which the periphery of the wheel is used.

Our Technical Department is able to give advice on all wheel forming queries.

THE CHURCHILL MACHINE TOOL CO. LTD.
BROADHEATH MANCHESTER

THE ENGINEERS' DIGEST

Published Monthly by Engineers' Digest Ltd., 120 Wigmore Street, London, W.1. Tel.: WELBECK

ANNUAL SUBSCRIPTION OF 12 NUMBERS, £2 2s. :: SINGLE COPIES, 4s.

ADVISORY COMMITTEE

J. F. ALCOCK, B.A., M.I.Mech.E.
R. W. ALLOTT, M.A., A.R.Ae.S.
E. ALTON, D.Eng., A.M.Inst.B.E.
R. W. AYERS, M.I.W.
Col. J. BOWDEN, M.Inst.C.E., M.I.Mech.E.
H. H. BROUGHTON, M.I.Mech.E.
F. BUCKINGHAM, B.Sc., A.M.Inst.C.E., A.M.I.Mech.E., A.M.I.E.E.
T. H. BURNHAM, B.Sc. (Lond.), A.M.I.Mech.E.
J. S. CASWELL, M.Sc., M.I.Mech.E.
G. C. SAFFERY COOPER.
J. DICK, Ph.D., B.Sc., A.M.I.Mech.E.
D. FIFE, M.I.Mech.E.
G. E. FOXWELL, D.Sc. (Lond.), F.Inst.P., F.Inst.F., M.Inst.Gas.E.
R. GRIFFITHS, M.Sc.
H. HEYWOOD, Ph.D., M.Sc. (Eng.), M.I.Mech.E.
O. HURST, M.Inst.N.A.
Capt. J. S. IRVING, M.I.Mech.E., M.I.A.E., A.F.R.Ae.S., M.S.A.E.
F. C. JOHANSEN, M.Sc. (Eng.), M.I.Mech.E., F.R.Ae.S., M.I.Loco.E.
W. J. KEARTON, D.Eng., M.I.Mech.E., A.M.Inst.N.A.
Prof. W. KERR, Ph.D., M.I.Mech.E.
G. V. LOMONOSOFF, Dr.Ing., M.I.Mech.E.
B. J. LYMER, M.I.Mech.E.
D. T. MACIVOR, M.I.Mech.E., M.Cons.E.
W. O. MANNING, F.R.Ae.S.
R. B. MATTHEWS, Wh.Ex., A.M.Inst.C.E., M.I.E.E., F.R.Ae.S.
Prof. A. L. MELLANBY, D.Sc., LL.D., M.I.Mech.E.
J. H. R. RATCLIFFE, B.Sc. (Eng., M.I.Mech.E.
Col. C. W. D. ROWE.
W. A. SCOBLE, D.Sc., A.R.C.Sc., M.I.Mec
P. W. SEEWER, D.E. (Zurich), M.Inst.C. M.I.Mech.E.
Prof. S. PARKER SMITH, D.Sc., M.I. A.M.Inst.C.E.
C. E. H. VERITY, A.M.Inst.C.F., A.M.I. A.M.I.Mech.E.
E. G. WALKER, F.C.G.I., B.Sc. (E M.Inst.C.E., M.I.Mech.E., M.A.Sc.
Major F. L. WATSON, M.I.C.E., M.I.Mec
G. WATSON, M.Inst.C.E., M.I.Mech.E.
C. H. WOODFIELD, M.I.Mech.E., M.I.Struc
T. WRIGHT, Ph.D., M.Sc.
M. L. YATES, Ph.D., M.Sc.Tech., M.A.(Ca M.I.Mech.E.

ADVISORY COMMITTEE OF THE AMERICAN EDITION

Chairman: DR. ALEXANDER KLEMIN, New York University
R. S. ARCHER, Climax Molybdenum Company.
Prof. O. W. BOSTON, University of Michigan.
Dr. W. H. CARRIER, Carrier Corporation.
R. W. CARSON, Instrument Specialties Co., Inc.
Dr. L. W. CHUBB, Westinghouse Electric Corp.
A. E. RICHARD DE JONGE, Babcock & Wilcox Co.
Dr. O. S. DUFFENDACK, North American Phillips Co.
HANS ERNST, Cincinnati Milling Machine Co.
R. D. EVANS, The Goodyear Tire & Rubber Co.
CHRISTIAN E. GROSSER, Standard Machinery Co.
GEORGE F. HABACH, Worthington Pump & Machinery Corp.
Dr. VICTOR O. HOMERBERG, The Nitralloy Corp.
HERBERT R. ISENBURGER, St. John X-ray Service.
J. B. JOHNSON, A. A. F., Wright Field.
CHARLES M. JONES, John A. Roebling's Sons Co.
H. MANDEL, The Wickman Corp.
J. C. MATHES, Dow Chemical Co.
H. W. McQUAID, Republic Steel Corp.
R. F. MILLER, Carnegie-Illinois Steel Corp.
Professor L. F. MOODY, Princeton University.
Professor H. F. MOORE, University of Illinois.
LAWRENCE OTTINGER, United States Plyw Corp.
C. E. PRITCHARD, Republic Steel Corp.
JOHN SANDS, International Nickel Co.
JAMES G. SAWYER, Buffalo Turbine Corp.
Dr. A. O. SCHMIDT, Kearney & Trecker C
L. K. SILLCOX, New York Air Brake Co.
ALBERT F. SPERRY, President, Instru Society of America.
R. DAVID THOMAS, JR., Arcos Corp.
GEORGE A. TINNERMAN, Tinnerman Produ Inc.

INVESTIGATION OF HEAT TRANSFER AND FRICTION LOSS FOR STATIONARY FLOW AT ULTRA-HIGH VELOCITIES

By N. V. ILUCHIN. (From *Izvestia Akademii Nauk U.S.S.R.*, No. 5, 1946, pp. 703-718, 13 illustrations.)

IN recent years the problems of heat transfer and flow resistance for the flow of gases at ultra-high velocities have assumed considerable importance. In 1934 the author carried out a number of experiments concerning the heat transfer from air at high flow velocity, and established the interrelationship between Nusselt-numbers and Péclet-numbers for values of *Pe* ranging from 65,000 to 270,000 for velocities approaching the velocity of sound. These experiments were carried out at low temperature levels (about 300 deg. C.), and air instead of flue gas was employed as the flow medium.

In 1936 the author conducted a number of tests relating to the study of the laws of heat transfer prevailing at ultra-high velocities for the flow of flue gases. For this purpose a combustion chamber was built in which mazout was burned under pressure. The results of these tests were analytically evaluated, but the investigation of the flow resistance prevailing in the presence of heat exchange proved inconclusive. Also the problem of the influence of the temperature factor remained unsolved. In 1936, I. Jung* published the results of his experimental investigation of heat transfer and flow resistance for the case of high velocity gas flow. He suggested a mathematical formulation including the temperature factor. In 1939 V. Leltshuk carried out an experimental investigation of the heat transfer from a stream of air. His findings agree well with those obtained by the author in 1934.

An analysis of the mathematical formulæ suggested by various authors leads to the conclusion that the problems of the influence of the ratio l/d upon the coefficient of heat transfer are not yet solved and it is for this reason that the author undertook a series of tests conducted on tubes having different l/d ratios. If Jung's results are compared with the Nusselt formula, then Nusselt's formula, which was established in 1917, will indicate a greater influence of the temperature factor than that author's formula established in 1930. According to Groeber's investigations the coefficient of heat transfer will fall with increasing gas temperature, but this conclusion is opposed by other authors ; and Schulze was unable to discover any influence of the temperature factor upon the coefficient of heat transmission.

A strict consideration of the problem on the basis of the theory of similarity leads to the conclusion that the characteristic criteria must contain a temperature factor. But in practice it is widely considered permissible to exclude the temperature factor. Considering the wide divergence existing between the findings of the various investigators with regard to the influence of the temperature factor the author decided to undertake the following investigations *to wit :* (a) Establishment of a theory of heat transfer and flow resistance, this theory to cover a wide range of Reynolds numbers and temperature factors, (b) Experimental verification of such a theory and the establishment of numerical relationships, and (c) Examination of the influence of the ratio l/d and of the criterion *Ba* upon heat transfer and flow resistance.

THEORETICAL INVESTIGATION.

The tangential stress in turbulent flow of any kind is expressed by

$$\tau = \mu' \frac{du}{dy} \quad .. \quad .. \quad (1)$$

where the factor μ' is called the coefficient of turbulence.

According to Nusselt it can be assumed that

$$\mu' = c_0 \mu \left(\frac{\rho \cdot u \cdot y}{\mu} \right)^n \quad .. \quad .. \quad (2)$$

where n is an exponent the magnitude of which is determined by the range of Reynolds numbers concerned, u is the velocity of flow, y is the distance of the point considered from the tube wall, μ is the kinematic viscosity, ρ is the density of the gas, and c_0 is a numerical constant. For an infinitely small volume of gas contained in the length dl of a tube of the diameter $2r$, it is

$$F\,dp + F\rho w\,dw + 2\tau_{\text{WALL}}\pi r\,dl = 0 \quad .. \quad (3)$$

where τ_{WALL} is the wall friction force, $F = \pi r^2$ is the cross-sectional area of the tube and w is the mean velocity of flow. It will be assumed that the tangential stress distribution over the tube section may be represented with sufficient accuracy by the linear relationship

$$\frac{\tau}{\tau_{\text{WALL}}} = \frac{r-y}{r}$$

It can therefore be written

$$dp + \rho w\,dw + \frac{2c_0}{r-y}\mu\left(\frac{\rho \cdot u \cdot y}{\mu}\right)^n \frac{du}{dy}\,dl = 0 \quad (4)$$

On the other hand it is

$$dp + \rho \cdot w \cdot dw + \xi \frac{w^2}{4r} \cdot \rho \cdot dl = 0 \quad .. \quad (5)$$

where ξ is the coefficient of hydraulic friction. By introducing

$$x = \frac{y}{r} \text{ and } z = \frac{u}{w}$$

we obtain from formulæ (4) and (5) the expression :

$$c_0 \cdot K \cdot z^n \cdot dz = \frac{1-x}{x^n}\,dx \quad .. \quad (6)$$

where $$\frac{16}{A_1\,2^n} Re^{m+n-1} = K$$

In the latter expression the factor A_1 is a constant. By integrating equation (6) we obtain

$$\frac{c_0}{n+1} K z^{n+1} = \frac{1}{1-n} x^{1-n} - \frac{1}{2-n} x^{2-n} + C \quad (7)$$

where C is an undetermined constant. At the tube wall it is $z = 0$ and $C = 0$; while in the centre of the tube, where $x = 1$, it obtains

$$c_0 K = \frac{n+1}{(1-n)(2-n)} \frac{1}{z_{\max}^{n+1}}$$

where $$z_{\max} = \frac{u_{\max}}{w}$$

in the latter expression $u_{\max}$ signifies the velocity of flow prevailing in the centre of the tube. Consequently it is

$$u = u_{\max} \cdot (2-n)^{\frac{1}{1+n}} x^{\frac{1-n}{1+n}} \left(1 - \frac{1-n}{2-n} x\right)^{\frac{1}{1+n}} \quad (8)$$

* Forschungsheft No. 380, 1936.

This equation yields the distribution of the velocity of flow over the tube section. In order to be able to determine the value for c_0, some assumption regarding the functionality of the frictional force must be made. Within the range of Reynolds numbers extending from $Re = 10^5$ to $Re = 10^6$ the friction coefficient can be expressed by

$$\xi = \frac{A_1}{Re^m}$$

On the basis of the formula given by Nikuradse, and considering the range of Reynolds numbers given above, it will be $A_1 = 0{\cdot}139$ and $m = 0{\cdot}18$, so that

$$\xi = \frac{0{\cdot}139}{Re^{0{\cdot}18}}$$

From equations (6) and (7) the relationship between w and u_{max} is found as

$$u_{max} = w \left[\frac{1+n}{(1-n)(2-n)} \frac{A_1 2^n}{16 c_0} \right]^{\frac{1}{1+n}} Re^{\frac{1-m-n}{1+n}} \quad (*)$$

Within the range of Reynolds numbers considered the profile of the velocity distribution is not very pronounced and the ratio u_{max}/w remains therefore approximately constant. In view of this fact the exponent of Re as given in the equation (*) will be little different from zero and it may therefore be assumed that

$$l - m - n = 0 \text{ and consequently } n = 0{\cdot}82$$

and

$$u_{max} = \frac{1}{1{\cdot}095} \left(\frac{0{\cdot}155}{c_0} \right)^{0{\cdot}55} . w \quad .. \quad (9)$$

Equation (8) can also be written thus :

$$u = 1{\cdot}095\, u_{max}\, x^{0{\cdot}1} (1 - 0{\cdot}152\, x)^{0{\cdot}55} \quad .. \quad (10)$$

The numerical value for the coefficient c_0 can be determined as follows : The mean velocity of flow is expressed by the equation

$$w = 2 \int_0^1 u (1 - x)\, dx.$$

By introducing the value for u as given in formula (10) and combining with equation (9) it becomes

$$w = 2 \int_0^1 (1 - x)\, w \left(\frac{0{\cdot}155}{c_0} \right)^{0{\cdot}55} x^{0{\cdot}1} (1 - 0{\cdot}152\, x)^{0{\cdot}55}\, dx$$

or

$$\frac{1}{2} \left(\frac{c_0}{0{\cdot}155} \right)^{0{\cdot}55} = \int_0^1 x^{0{\cdot}1} (1 - x)(1 - 0{\cdot}152\, x)^{0{\cdot}55}\, dx.$$

This yields by integration : $c_0 = 0{\cdot}113$.

Once c_0 has been determined, the relationship between maximum and mean velocity of flow in the tube can be found from equation (9) as

$$\frac{u_{max}}{w} = 1{\cdot}088$$

or

$$\frac{w}{u_{max}} = 0{\cdot}92 \quad .. \quad .. \quad (11)$$

The equation (10) can also be written in the form

$$u = 1{\cdot}19\, w\, x^{0{\cdot}1} (1 - 0{\cdot}152\, x)^{0{\cdot}55} \quad .. \quad (12)$$

Equation (8) represents correctly the distribution of the velocity of flow throughout the flow area of the tube except for the laminar boundary flow ; in fact it yields a rather interesting result which deserves attention.

An examination will now be made of the flow under conditions of heat transfer. The density ρ of the fluid and the kinematic viscosity μ are functions of the temperature, and their numerical values will change over the tube section. Consequently it is necessary to insert into equation (2) the density and viscosity values as they exist at the point under consideration.

If Θ_{WALL} represents the absolute wall temperature, Θ is the absolute temperature of the gas, $\bar{\Theta}$ is the mean absolute temperature over the section, $\Delta\bar{\Theta}$ is the mean temperature difference, and $\Delta\Theta$ is the temperature difference, then

$$\Delta\Theta = \Theta - \Theta_{WALL} \text{ and } \Delta\bar{\Theta} = \bar{\Theta} - \Theta_{WALL}.$$

It will be assumed that the velocity distribution curve according to (8), prevailing under conditions of adiabatic flow, be valid also for flow in the presence of heat transfer. This assumption, which applies to conditions of developed turbulence, must be confirmed either by experiment or by comparing the theoretical conclusions with available test data.

The assumption that similarity exists between the temperature and the velocity fields leads to the basic concept that

$$\frac{u}{u_{max}} = \frac{\Delta\Theta}{\Delta\Theta_{max}} \quad .. \quad .. \quad (**)$$

or $\frac{u}{w} = \frac{\Delta\Theta}{\Delta\bar{\Theta}}$, and in this case the following relationship will prevail :

$$\alpha = \frac{g \,.\, C_p}{w} \,.\, \tau_{WALL} = \frac{\lambda}{\mu \,.\, w} \,.\, \tau_{WALL} \quad .. \quad (13)$$

Here α is the coefficient of heat transfer, and C_p is the specific heat at constant pressure. By assuming the Prandtl number to be unity, it becomes

$$\frac{g\, C_p\, \mu}{\lambda} = 1 \quad .. \quad .. \quad (14)$$

and it therefore is

$$\Theta = \Theta_{WALL} \left(1 + \frac{\Delta\bar{\Theta}}{\Theta_{WALL}} \frac{\mu}{w} \right) \quad .. \quad .. \quad (15)$$

By making $\frac{\Delta\bar{\Theta}}{\Theta_{WALL}} = \varphi$ we have

$$\Theta = \Theta_{WALL} \left(1 + \varphi \frac{u}{w} \right) \quad .. \quad .. \quad (15')$$

The density of the gas as related to the temperature of the tube wall will be denoted by ρ_{WALL} and the density ρ of the gas for the stream temperature will be

$$\rho = \rho_{WALL} \frac{\Theta_{WALL}}{\Theta} \quad \text{or} \quad \rho = \rho_{WALL} \frac{1}{1 + \varphi \frac{u}{w}}$$

The variation of the kinematic viscosity with the temperature can be expressed by

$$\mu = \mu_{WALL} \left(\frac{\Theta}{\Theta_{WALL}} \right)^{m_1}$$

or

$$\mu = \mu_{WALL} \left(1 + \varphi \frac{u}{w} \right)^{m_1}$$

By combining equations (4) and (5) it obtains

$$\xi \frac{w^2}{4r} \bar{\rho} = \frac{2 c_0 \mu}{r - y} \left(\frac{u y \rho}{\mu} \right)^{0.82} \frac{du}{dy} \quad .. (16)$$

where $\bar{\rho}$ is the density of the gas averaged over the flow area, while ρ, μ and u are density, viscosity, and flow velocity respectively prevailing at any given point. By introducing the expressions for ρ and μ into formula (16), we have

$$\frac{z^{0.82}\, dz}{(1 + \varphi z)^{(0.82 - 0.18 m_1)}} = \frac{\bar{\rho}\, \xi\, Re_{WALL}^{0.18} (1 - x)\, dx}{\rho_{WALL}\, 8\, c_0\, 2^{0.18} \cdot x^{0.82}} \quad (17)$$

Here it is $Re_{WALL} = \dfrac{\rho_{WALL} \cdot w \cdot d}{\mu_{WALL}}$

By integration :

$$\int_0^x \frac{\bar{\rho}\, \xi\, Re_{WALL}^{0.18} (1 - x)}{\rho_{WALL}\, 8\, c_0\, 2^{0.18}\, x^{0.82}}\, dx =$$

$$= 5.45 \frac{\bar{\rho}}{\rho_{WALL}} \xi\, Re_{WALL}^{0.18} \cdot x^{0.1^{*}} (1 - 0.153\, x).$$

We make $\quad \overline{H} = 5.45\, \xi\, Re_{WALL}^{0.18} \dfrac{\bar{\rho}}{\rho_{WALL}} \quad (***)$

and obtain :

$$\int_0^z \frac{z^{0.82}\, dz}{(1 + \varphi z)^{(0.82 - 0.18 m_1)}} = \overline{H} (1 - 0.153\, x)\, x^{0.18} \quad (18)$$

By making use of Jung's statement that $\mu \approx c\, T^{0.64}$ for combustion products in the range from 200 deg. C. to 1,200 deg. C., and by making $m_1 = 0.64$, we have

$$\overline{H} (1 - 0.153\, x)\, x^{0.18} = \int_0^z \frac{z^{0.82}\, dz}{(1 + \varphi \cdot z)^{0.705}} \quad (19)$$

The relationship between H and φ can be determined by means of equation (19). By solving the integral in equation (19) by the approximate method according to Gauss, we find

$$\overline{H} = \frac{0.755}{(1 + \varphi)^{0.52}} \quad .. \quad .. (20)$$

This expression for $\overline{H}$ can be introduced into equation (***) and the friction coefficient will then be found as

$$\xi = \frac{0.139}{\overline{Re}_{WALL}^{0.18}} \left(\frac{\bar{\theta}}{\Theta_{WALL}} \right)^{0.3} \quad .. \quad .. (21)$$

where

$$\overline{Re}_{WALL} = \frac{\bar{\rho} \cdot w \cdot d}{\mu_{WALL}}$$

This expression represents the fundamental equation for the coefficient of flow resistance, taking into account the temperature factor. For adiabatic flow in which $\theta = \Theta_{WALL}$, equation (21) takes the form of the well known Nikuradse equation for the range of Reynolds numbers considered.

If the expression for ξ is introduced into equation (13), in which it can obviously be made

$$\tau_{WALL} = \frac{\xi}{8} \bar{\rho}\, w^2 \quad \therefore \quad .. (22)$$

then we have

$$Nu_{WALL} = 0.0174\, Pr_{WALL}^{0.18}\, Pe_{WALL}^{0.82} \left(\frac{\bar{\theta}}{\Theta_{WALL}} \right)^{0.3} \quad (23)$$

The formulæ (21) and (23) can be employed for the computation of heat exchange and flow resistance in the case of the flow of gases through tubes, and they are valid for Reynolds numbers up to $Re = 10^6$.

In the theoretical investigation of the similarity of temperature and velocity fields, the temperature of throttling must enter into the right hand side of the equation $u/w = \Delta\Theta/\Delta\bar{\theta}$. This temperature has a simple physical meaning. For adiabatic throttling it corresponds to the total conversion of kinetic energy of the gas into heat. Side by side with this temperature exists the thermodynamic temperature to which all physical constants must be referred to. The difference between these two temperatures is the ratio of the thermal equivalent of the kinetic energy to the specific heat ; and it therefore varies with the square of the velocity. It is for this reason that for gases flowing at low velocity, there exists practically no difference between these two temperatures. The temperature of throttling appears in all equations of the thermodynamic theory of heat exchange, and only the physical constants contained in these equations must be related to the thermodynamic temperature.

EXPERIMENTAL INVESTIGATION.

All the aforementioned theoretical conclusions refer only to smooth tubing. The inside wall surface of the tubes tested was not subjected to any special finishing treatment, and only ordinary seamless steel tubing was investigated. It therefore became necessary to establish the coefficient of hydraulic friction for these tubes in order to allow a comparison of the test results with the formulæ for smooth tubes, and thus to establish the quality of the interior wall surface. The experimental method for the determination of the coefficient of hydraulic friction does not represent any particular difficulty, and therefore it is not discussed here. For technical reasons a Reynolds number of 10^5 was not exceeded in these experiments, and the value of the coefficient of hydraulic friction can therefore be compared with values based upon Blasius' formula. Under these conditions roughness of the tube wall was not discovered. It is true that the tests were conducted at Reynolds numbers far exceeding the range of validity of Blasius' formula, but even so the influence of wall roughness, if present, could be expected to make itself felt. Therefore it is permissible to assume that the internal wall surface of the tubing investigated was technically smooth without having undergone any special finishing process.

The salient features of the experimental installation constructed for the purpose of carrying out the various tests is outlined in Fig. 1. Here it will be seen that the flue gases are passed from the combustion chamber into a duct from which part of the gases is passed into the convection elements for the study of the problems referred to, while the rest of the gases is ejected direct to atmosphere. As will be seen from the diagram, the installation for the study of heat transfer and friction loss consists of two convection tubes of identical shape but of l/d ratios of 96·5 and 62·4 respectively. The design and arrangement of these two tubes is shown in more detail in Fig. 2.

During the starting period all the flue gas is discharged to atmosphere through the exhaust pipe ; this is done in order to prevent overheating of the installation. In front of the inlets of the convection tubes an ante-

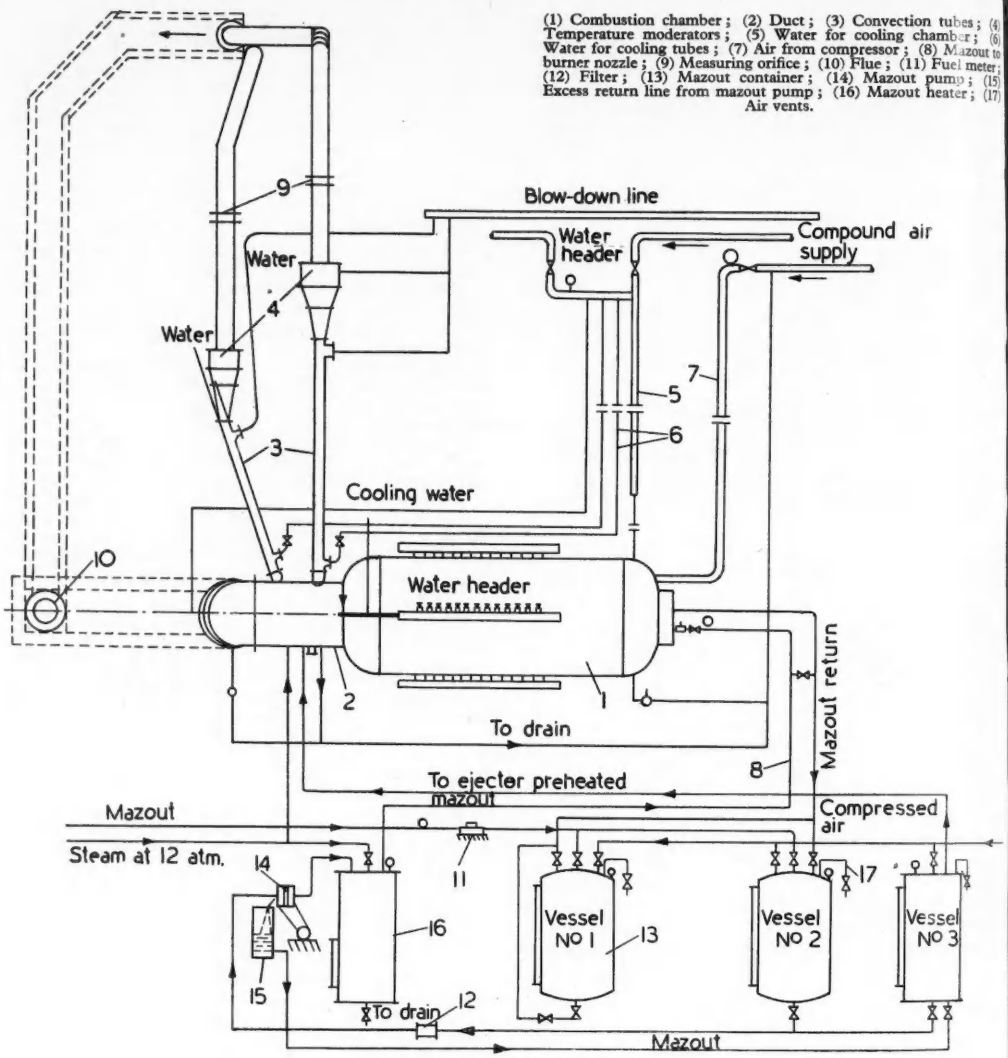
(1) Combustion chamber; (2) Duct; (3) Convection tubes; (4) Temperature moderators; (5) Water for cooling chamber; (6) Water for cooling tubes; (7) Air from compressor; (8) Mazout to burner nozzle; (9) Measuring orifice; (10) Flue; (11) Fuel meter; (12) Filter; (13) Mazout container; (14) Mazout pump; (15) Excess return line from mazout pump; (16) Mazout heater; (17) Air vents.
Blow-down line
Water header
Compound air supply
Water
Water
Cooling water
Water header
To drain
Mazout return
To ejecter preheated mazout
Mazout
Steam at 12 atm.
Compressed air
Vessel No 1
Vessel No 2
Vessel No 3
To drain
Mazout

Fig. 1. **General diagram of test plant.**

chamber is provided to enable measurement of the temperature of the expanding gases to be made before the gases enter the convection tubes. As will be seen from Fig. 2, provision is also made to measure the pressure in the tube and the temperature of the tube wall at a number of points along the tubes. In the expanding part of the diffuser thermocouples are provided for measuring the temperature of the expanded gas.

As one of the tasks consisted in the determination of the temperature influence, a series of tests at various temperatures had to be made. In each series of tests, conducted at various flow rates, the temperature and with it the temperature factor had to be kept constant, and the pressure in the combustion chamber was also kept constant. This was achieved by appropriate control of fuel supply and air supply. The gas temperature in the gas duct was measured by means of the pyrometer installation outlined in Fig. 3.

The temperatures of the gases before and after the convection tubes were measured by means of specially designed thermocouples as shown in Fig. 4. The tube wall temperature was measured by means of thermocouples of 0·1 mm. diameter arranged as shown in Fig. 5. The measurement of the temperature at the tube surface and in the laminar layer is very difficult of execution, and this temperature was therefore computed instead, the computation being based on the hydrodynamic theory of heat exchange. The Péclet and Reynolds numbers were established according to the formulæ

$$\overline{Pe}_{WALL} = \frac{4}{\pi d} G \frac{C_{p\,WALL}}{\lambda_{WALL}}$$

$$\overline{Re}_{WALL} = \frac{4}{g\,\pi\,3600} \frac{1}{\mu_{WALL}} G$$

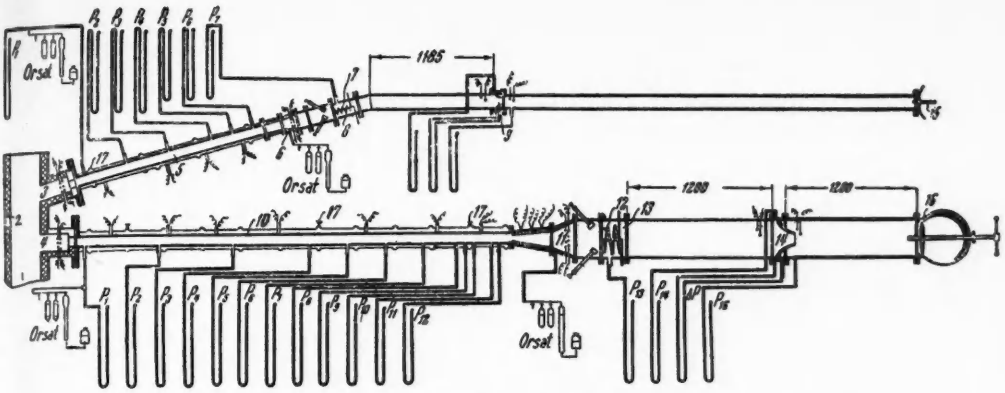

Fig. 2. **Diagram of convection tube installation.**

(1) Duct; (2) Peephole; (3) Ante-chamber of small convection tube; (4) Ante-chamber of large convection tube; (5) Small convection tube; (6) (11) Diffuser; (7) (12) Coils; (8) (13) Temperature moderator; (9) (14) Measuring orifice; (10) Large convection tube; (15) Throttle of small convection tube; (16) Throttle of large convection tube; (17) Drain cock.

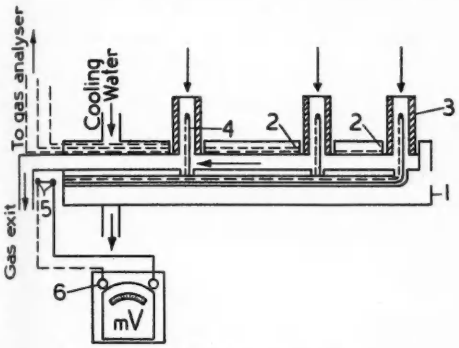

Fig. 3. **Pyrometer of three-junction type.**

(1) Pyrometer casing; (2) Gas intake from furnace; (3) Refractory tube; (4) Hot junction; (5) Cold junction; (6) Galvanometer.

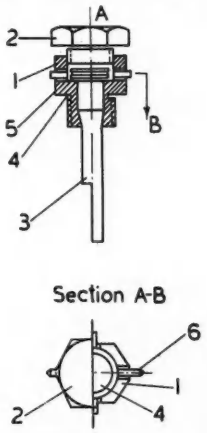

Fig. 4. **Plug for measuring gas temperature under pressure.**

(1) Body of plug; (2) Plug; (3) Porcelain bush; (4) Fibre washer; (5) Copper washer; (6) Mica bush.

in which all physical constants are referred to the measured wall temperature. Proceeding from theoretical considerations, equation (23) was selected for the interpretation of the test results, because this formula can be applied to any point of the tube area. The test results yielded the coefficient of heat transfer in the form of an average value for the length of section investigated. Comparison of the experimental values for the heat transfer coefficient must be carried out by integrating over the length of section, that is, by means of the expression

$$Nu_T = \frac{1}{L}\int_0^L \frac{0{\cdot}0174\,.\,Pr_{\text{WALL}}^{0{\cdot}18}\;\overline{Pe}_{\text{WALL}}^{0{\cdot}82}}{\Theta_{\text{WALL}}^{0{\cdot}3}}\,\bar{\Theta}^{0{\cdot}3}\,dl \quad (a_1)$$

In order to be able to solve this integral, the functional variation of the temperature over the length of section considered, must be known. For this purpose it will be assumed that logarithmic functionality between temperature and length of section exists. This can be expressed by

$$\Theta = \Theta_1\, e^{\ln\left(\frac{\theta_2}{\theta_1}\right)\frac{l}{L}} \quad .. \quad .. \quad (24$$

In this case the actual Nusselt number will be

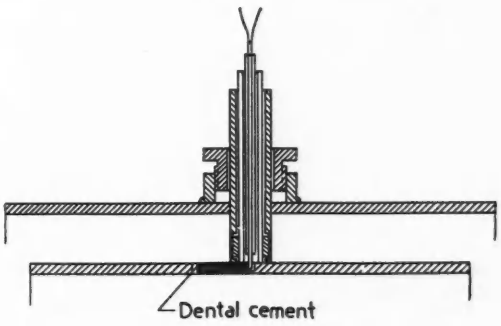

Fig. 5. **Thermocouple for measuring tube wall temperature.**

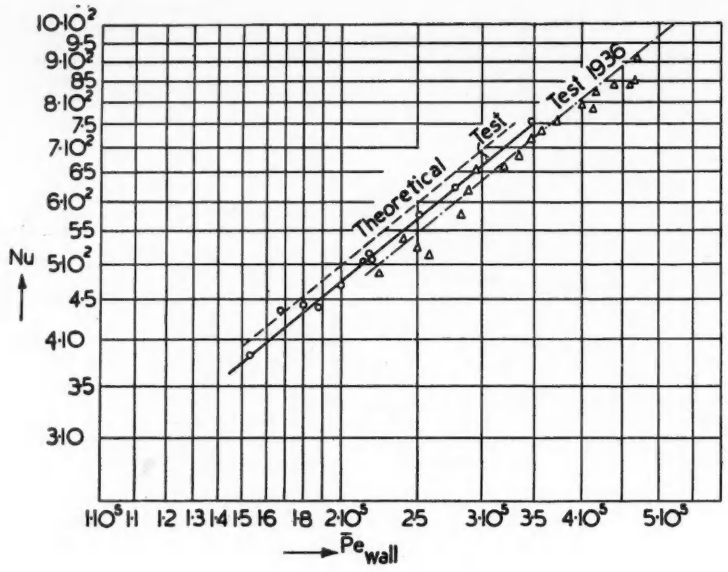

Fig. 6. **Relationship.**

$Nu = f(Pe)$ for $\frac{\theta_m}{\theta_{WALL}} = 2.52$

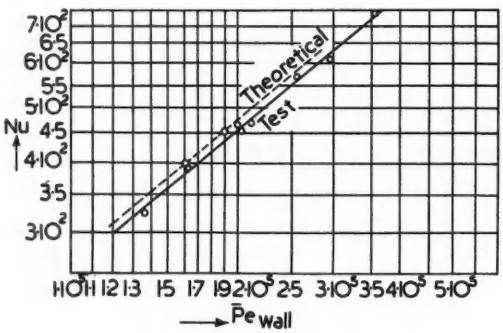

Fig. 7. **Relationship.**

$Nu = f(Pe)$ for $\frac{\theta_m}{\theta_{WALL}} = 2.33$

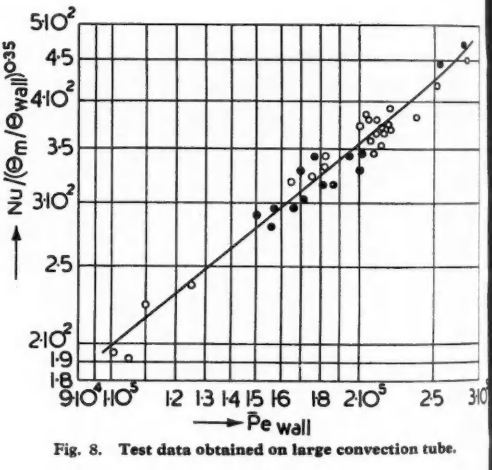

Fig. 8. **Test data obtained on large convection tube.**

$$Nu = 0{\cdot}0174\ Pr_{WALL}^{0{\cdot}18}\ \overline{Pe}_{WALL}^{0{\cdot}82}\left(\frac{\theta_1}{\theta_{WALL}}\right)^{0{\cdot}3}\ e^{0{\cdot}3\ln\left(\frac{\theta_2}{\theta_1}\right)\frac{l}{L}} \quad (25)$$

The mean Nusselt number can be obtained from equation (a_1) by combining equations (25) and (a_1) and then integrating. It thus obtains

$$Nu_T = 0{\cdot}0174\ Pr_{WALL}^{0{\cdot}18} \times \overline{Pe}_{WALL}^{0{\cdot}82} \frac{\left(\frac{\theta_1}{\theta_{WALL}}\right)^{0{\cdot}3}}{2{\cdot}303\log\left(\frac{\theta_2}{\theta_1}\right)^{0{\cdot}3}}\left[\left(\frac{\theta_2}{\theta_1}\right)^{0{\cdot}3}-1\right] \quad (26)$$

The original equation for the determination of the friction coefficient is

$$\frac{dw^2}{2g} = -v\,dp - \frac{\xi}{d}\frac{w^2}{2g}dl \quad .. \quad (27)$$

By introducing the quantity of flow, it results

$$\frac{G}{3600\,.\,g\,.\,F}dw = -dp - \xi\frac{G}{3600\,.\,2g\,.\,F\,.\,d}\,.\,w.\,dl \quad .. \quad (28)$$

If ξ is taken as constant, integration of equation (28) yields

$$\frac{G}{3600\,.\,g\,.\,F}(w_2 - w_1) = (p_1 - p_2) - \xi\frac{G}{2g\,.\,3600\,.\,F\,.\,d}\int_0^l w\,.\,dl \quad .. \quad (29)$$

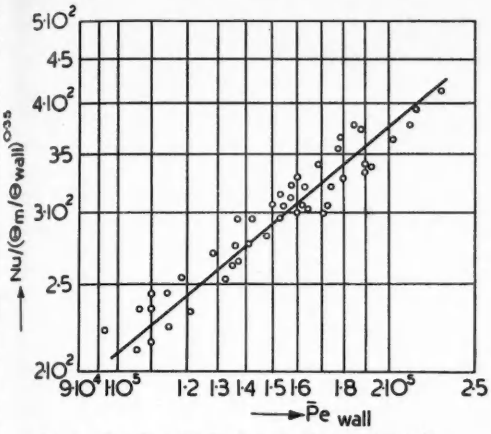

Fig. 9. **Test data obtained on small convection tube.**

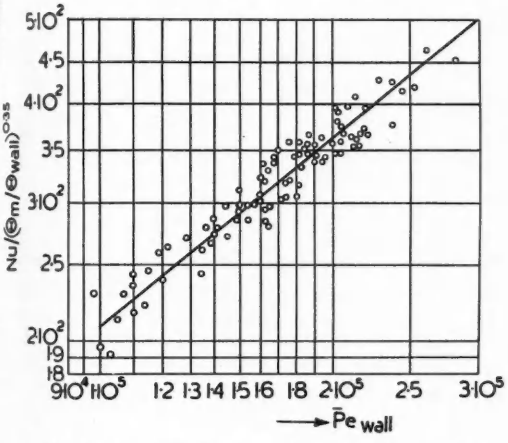

Fig. 10. **Combined graph for small and large convection tubes.**

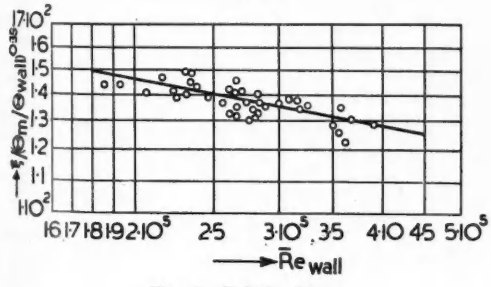

Fig. 11. **Relationship.**

$$\frac{\xi}{(\theta_m/\theta_{WALL})^{0.35}} = f(\overline{Re}_{WALL})$$

The integral $\int_0^l w \cdot dl$ can be evaluated by planimetric evaluation of the curve which represents the velocity variation. The coefficient of friction is then determined from equation (29). In order to find the velocity in a given section of the tube, the simple equation

$$w^2 + \frac{2gC_p \cdot F}{ARG} pw - \frac{2g}{A} C_p \Theta = 0 \quad .. \quad (30)$$

is used.

ANALYSIS OF TEST DATA.

The relationship $Nu = f(Pe)$ as it was found from the tests conducted with the ratio $\Theta_m/\Theta_{WALL} = 2{\cdot}52$ is charted in Fig. 6. The latter diagram also gives the corresponding data found by the author in 1936 ; and it will be seen that the divergence does not exceed 4 per cent. Moreover, this graph shows that the experimental values of the heat transfer coefficient agree with the computed values, the maximum discrepancy between the two not exceeding 3 per cent. The test data obtained for the ratio $\Theta_m/\Theta_{WALL} = 2{\cdot}33$ are charted in Fig. 7 which likewise shows satisfactory agreement between theoretical and experimental values. In Fig. 8 is charted the relationship

$$\frac{Nu}{(\Theta_m/\Theta_{WALL})^{0.35}} = f(\overline{Pe}_{WALL})$$

as found in the present investigation and in the tests made with air in 1934. Fig. 9 shows the corresponding data for the tests made with the use of the smaller convection tube. The graphs Figs. 8 and 9 can be expressed by the equation

$$Nu_z = A_0 \overline{Pe}_{WALL}^{0.82} \left(\frac{\Theta_m}{\Theta_{WALL}}\right)^{0.35} \quad .. \quad (31)$$

where it is $A_0 = 0{\cdot}0161$ for the tests conducted with the large convection tube and $A_0 = 0{\cdot}0164$ for those made with the small tube. Fig. 10 combines the results found with the two convection tubes. The functionality charted can be expressed by a formula similar to formula (31), and in this case it will be $A_0 = 0{\cdot}0162$. This result enables the conclusion to be drawn that the ratio l/d does not affect the coefficient of heat transfer, and it is therefore proposed to express the heat transfer coefficient by the relationship

$$Nu_z = 0{\cdot}0162\, \overline{Pe}_{WALL}^{0.82} \left(\frac{\Theta_m}{\Theta_{WALL}}\right)^{0.35} \quad .. \quad (32)$$

A comparison of the author's formula with that given by Jung shows that the Nusselt number as given by Jung is larger than that of the author, the discrepancy amounting to some 20 per cent. From the various test results the author concludes that the friction loss in the tube can be expressed by

$$\frac{\xi}{(\Theta_m/\Theta_{WALL})^{0.35}} = f(\overline{Re}_{WALL}).$$

The influence of the temperature factor upon the friction coefficient is established in the graph given in Fig. 11. From this graph the functionality of the friction coefficient can be established as

$$\xi = \frac{0{\cdot}131}{\overline{Re}_{WALL}^{0.18}} \left(\frac{\Theta_m}{\Theta_{WALL}}\right)^{0.35} \quad .. \quad .. \quad (33)$$

where

$$\overline{Re}_{WALL} = \frac{\gamma \cdot w \cdot d}{g \cdot \mu_{WALL}}$$

This formula is in full agreement with the theoretical findings, and the values for the friction coefficient as found by the author agree within 3·5 per cent with the data established by Jung.

BELGIUM

ELASTIC ABSORPTION OF TEMPERATURE DISTORTIONS IN PLANE PIPE SYSTEMS

By A. SCHLAG and A. JORISSEN. (From *Revue Universelle des Mines*, Vol. 90, No. 1, 1947, pp. 10-20, 13 illustrations.)

I. INTRODUCTION

INDUSTRIAL pipe systems for conveying fluids at high temperatures and pressures are subject to stresses which can be confined within allowable limits by the means of fixing, so that only reasonable distortions are possible due to expansions and contractions. The pressure of the fluid and the weight and shape of the pipe line, are factors deciding the positioning and condition of the means of fixing, and the following considerations relate to systems in which stresses are determined by them. They apply particularly to pipe layouts in which the design and construction obtains the heat rigidity wherever essential, and the maximum relief of stress where the pipe is curved or bent.

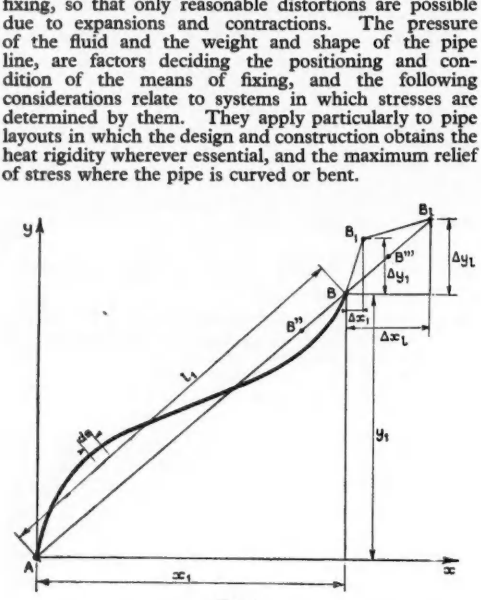

Fig. 1.

If a pipe system AB (Fig.1) is subjected to a temperature variation Δt the end point B is liable to displacement to a point B_l if A is fixed.

The displacement

$$BBl = \alpha . \Delta t . l_1 \quad .. \quad .. \quad (I, 1)$$

when α is the coefficient of expansion and l_1 is the distance between A and B.

If x_1 and y_1 are the co-ordinates of B the co-ordinates of the displacement are :

$$\left.\begin{aligned} \Delta x_l &= \alpha . \Delta t . x_1 \\ \Delta y_l &= \alpha . \Delta t . y_1 \end{aligned}\right\} \quad .. \quad (I, 2)$$

B however is restrained and not free to be displaced to B_l and therefore the expansion of the pipe must take place by bending between A and B and the alignment of these two points of the pipe length will be deviated to suit this condition. B will be misaligned with respect to A by Δx_1 and by Δy_1 with respect to B_l, and an effort is therefore required to produce this with co-ordinates

$$-(\alpha . \Delta t . x_1 - \Delta x_1); \quad -(\alpha . \Delta t . y_1 - \Delta y_1)$$

Thus, whereas the freely expanded pipe would retain its alignment to point B_l, the fixed point B reacts against the force due to expansion and the pipe must deviate from the straight line between A and B.

PRESTRESSED MOUNTINGS

To compensate for distortions of a pipe line due to temperature differences it can be mounted in a state of tension, and if the extension for this purpose is equal to the length of the pipe between fixing is due to expansion under maximum temperature, the stresses in the pipe will be reduced by 50 per cent.

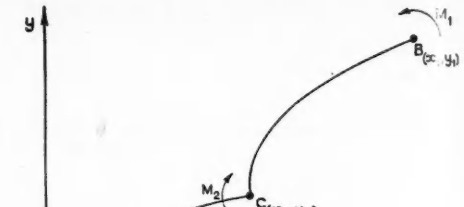

Fig. 2.

II. GENERAL EQUATIONS

If a pipe system has an intermediate hinged support (see Fig. 2), and when end A is fixed, a small movement of B to B_1 may still occur having components Δx_1 and Δy_1. The moment of force necessary at the supports to obtain deformations in the pipe resulting from expansion are :

$$\Delta x_1 - \alpha . \Delta t . x_1; \quad \Delta y_1 - \alpha . \Delta t . y_1; \quad \omega_1 - \omega_0$$

The value of these deformations is given by the general equations relative to a hyper-static system (Bresse's equations) [5].

$$\omega_1 - \omega_0 = \int_A^B \frac{k M}{E I} ds + \omega_2 \quad .. \quad .. \quad (II, 1)$$

where ω_0, ω_1 and ω_2 are the rotations about A, B and C respectively.

$$\Delta x_1 - \alpha . \Delta t . x_1 = -\omega_1 . y_1 + \omega_2 . y_2 + \int_A^B \frac{kM}{EI} y \, ds \quad (II, 2)$$

$$\Delta y_1 - \alpha . \Delta t . y_1 = \omega_1 x_1 - \omega_2 x_2 - \int_A^B \frac{kM}{EI} x \, ds \quad (II, 3)$$

kI is the moment of inertia of the pipe cross-section under consideration, and I is the moment of inertia of the cross-section corresponding to the most common pipe dimensions of the system.

$$K_i = (-1)^i . EI . \omega^i / M_i, \quad i = 0, 1, 2. \ldots \quad (II, 4)$$

therefore (II, 1) can be written :

$$K_0 M_0 - K_1 . M_1 + K_2 . M_2 + \int_A^B kM \, ds = 0 \quad (II, 5)$$

in which M_0, M_1 and M_2 are the bending moments at A, B and C respectively.

If X and Y are the horizontal and vertical components of the supporting reaction at A, the components $-X$ and $-Y$ apply at B and consequently :

$$M = M_0 + Y . x - X . y = M_1 + Y . (x - x_1) - X . (y - y_1) \quad (II, 6)$$

From this the values of M at A, B and C can be derived. Using these values with (II, 5) and simplifying

$$M_0 (K_0 + K_1 + K_2 + s) + Y (K_1 x_1 + K_2 x_2 + sm) - X (K_1 y_1 + K_2 y_2 + sn) - 0 \quad .. \quad (II, 7)$$

in which

$$s=\int_A^B k\,ds;\quad s.m=\int_A^B k\,x\,ds;\quad s.n=\int_A^B k\,y\,ds \text{ (II, 8-10)}$$

Defining a and b :—

$$\left.\begin{aligned} a&=(K_1x_1+K_2x_2+sm)\,/\,(K_0+K_1+K_2+s)\\ \text{and}\quad b&=(K_1y_1+K_2y_2+sn)\,/\,(K_0+K_1+K_2+s)\end{aligned}\right\}\ \text{(II, 11)}$$

hence : $M_0 = X\,.\,b - Y\,.\,a$ .. .. (II, 12)

With co-ordinates (a, b) $M = 0$ at the central point O, and this is the centre of gravity of the system which consists of

(1) The trace of the pipe system ; in which each unit of length has a mass proportional to k.

(2) Concentrated masses K_0, K_1 and K_2 at points A, B and C.

As $M = 0$ the horizontal and vertical support reactions (a, b) are components of a " central force " through O.

To calculate the displacement of B with respect to A, the components are given by (II, 2), (II, 3) and (II, 4) as :

$$\Delta x_1-\alpha\,.\,\Delta t\,.\,x_1 = \frac{K_1M_1}{EI}\,y_1 + \frac{K_2M_2}{EI}\,y_2 + \int_A^B \frac{k\,M}{EI}\,y\,ds$$

$$\Delta y_1-\alpha\,.\,t\,.\,y_1 = -\frac{K_1M_1}{EI}\,x_1 - \frac{k_2M_2}{EI}\,x_2 - \int_A^B \frac{kM}{EI}\,x\,ds$$

The values of I_x and I_{xy} can now be defined by :—

$$I_x = K_1y_1^2 + K_2y_2^2 + \int_A^B k\,y^2\,ds \quad .. \text{ (II, 13)}$$

$$I_{xy} = K_1x_1y_1 + K_2x_2y_2 + \int_A^B k\,x\,y\,ds \;..\text{ (II, 14)}$$

in which I_x and I_{xy} represent the moments of inertia of the mass system with reference to the axes Ax, and A_x, A_y respectively.

Similarly we can define the moments and products of inertia with reference to two axes ξ and through the the central point parallel to Ax and $A\,y$.

Inserting appropriate values for the moments M

$$\Delta x_1-\alpha\,.\,\Delta t\,.\,x_1 = \frac{1}{EI}[YI_{\xi\eta} - XI_\xi] \;..\text{ (II, 15)}$$

$$\Delta y_1-\alpha\,.\,\Delta t\,.\,y_1 = \frac{1}{EI}[XI_{\xi\eta} - YI_\eta] \;..\text{ (II, 16)}$$

and inversely for the reactions :

$$Y = EI\,\frac{(\Delta x_1-\alpha\,.\,\Delta t\,.\,x_1)\,I_{\xi\eta} + (\Delta y_1-\alpha\,\Delta ty_1)\,I_\xi}{I_{\xi\eta}^2 - I_\xi\,.\,I_\eta} \quad \text{(II, 17)}$$

$$X = EI\,\frac{(\Delta x_1-\alpha\,\Delta tx_1)\,I_\eta + (\Delta y_1-\alpha\,\Delta ty_1)\,I_{\xi\eta}}{I_{\xi\eta}^2 - I_\xi\,.\,I_\eta} \quad \text{(II, 18)}$$

The angle between the central force and the x axis is

$$\tan\varphi = \frac{Y}{X}$$

Moment Diagram

As the reactions can be represented by a central force, the moments are simply given by the normal distance between the portion of the pipe under consideration and the central force F (Fig. 3).

It follows from this that :

(1) Points of inflexion, where the bending moment vanishes, are the points of intersection of the trace of the pipe and the central force ; and :

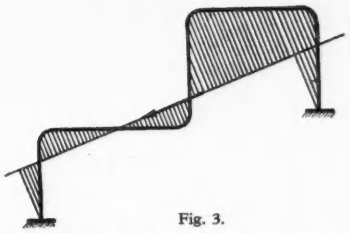

Fig. 3.

(2) If k is constant the maximum moments occur at those points of the pipe which are remotest from the line of the central force. If k is not constant the distances between the pipe and the central force representing the moments should be multiplied by $1/k$ if the portion of the pipe under the greatest stress is to be found.

III. PROPERTIES OF THE CENTRAL FORCE

(1) Taking any point D on the line of the central force, and drawing axes Dx' and Dy' through it parallel to $O\xi$ and $O\eta$ the moments and products of inertia $I_{x'}$ and $I_{x^1y^1}$ can be defined. It can be shown that :

$$Y\,.\,I_{\xi\eta} - X\,.\,I_\xi = Y\,.\,I_{x^1y^1} - X\,.\,I_{x^1} \;..\text{ (III, 1)}$$

The fundamental equations (II, 15) to (II, 18) therefore remain unaltered during the transition from (ξ, η) to the (x', y') system.

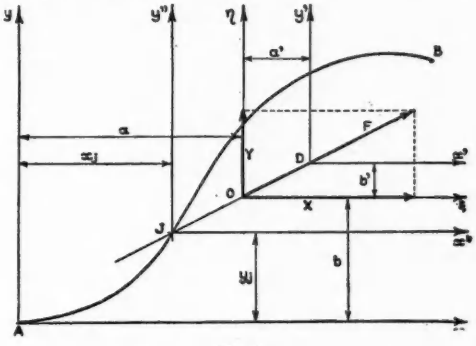

Fig. 4.

(2) The displacement of any point N of the pipe with the co-ordinates (x_n, y_n) can be calculated from general formulæ, for instance by the application of static moments according to Mohr[5]. The different components of the displacement are given by

$$\omega_N = \frac{K_0M_0}{E\,I} + \int_A^N \frac{k\,M}{E\,I}\,ds \quad .. \text{ (III, 2)}$$

$$\Delta x_n-\alpha\,\Delta t\,x_n = -\frac{K_0M_0}{EI}\,,yn + \int_A^N \frac{kM}{EI}\,yds - yn\int_A^N \frac{kM}{EI}\,ds \quad \text{(III, 3)}$$

and a similar equation obtained by replacing x by y.

(3) If a portion of the pipe system does not change its direction during the displacement $\omega_N = 0$;

$$\Delta x_n-\alpha\,\Delta t\,.\,x_n = \int_A^N \frac{kM}{EI}\,yds \quad .. \text{ (III, 4)}$$

also there is a similar equation for the y component.

It can be shown that the direction of the central force for the limited portion AN of the pipe system is the same as for the complete system AB.

(4) If there are several points of the pipe system

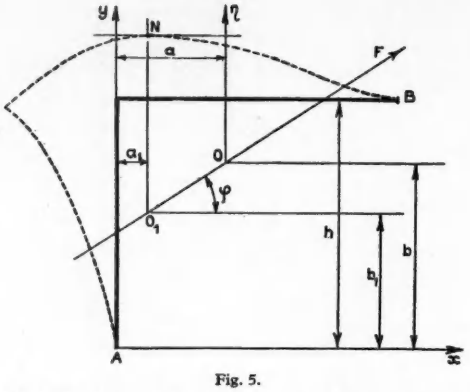

Fig. 5.

which remain parallel to their original direction, N being one of them :

$$\tan \varphi = (b - b_1) / (a - a_1) \; ; \quad .. \quad \text{(III, 5)}$$

in which (a_1, b_1) is the centre of gravity of the portion AN.

For example, for the system shown in Fig. 5

$$a_1 = \frac{\frac{x_n^2}{2}}{K_0 + h + x_n} \quad .. \quad \text{(III, 6)}$$

$$b_1 = \frac{\frac{h^2}{2} + h x_n}{K_0 + h + x_n} \quad .. \quad \text{(III, 7)}$$

$$\tan \varphi = \frac{b - \frac{h_2/2 + h x_n}{K_0 + h + x_n}}{a - \frac{x_n^2}{2(K_0 + h + x_n)}} \quad .. \quad \text{(III, 8)}$$

This relation gives x_n.

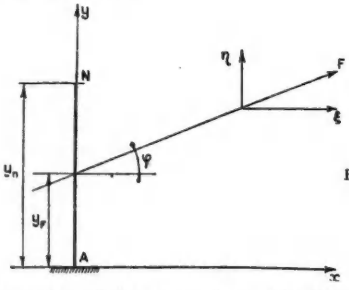

Fig. 6.

If a section of the system is straight (Fig. 6) and *encastré* at the end A

$$a_1 = 0, \quad b_1 = y_n / 2 \quad .. \quad \text{(III, 9)}$$

$$\tan \varphi = (b - \tfrac{1}{2} y_n) / a \quad .. \quad \text{(III, 10)}$$

on the other hand

$$\tan \varphi = (b - y_F) / a \quad .. \quad \text{(III, 11)}$$

and, consequently:

$$y_n = 2 y_F \quad .. \quad \text{(III, 12)}$$

(5) At points where the central force intersects with the trace of the pipe system $M = 0$. If $\mathcal{J}(x_j, y_j)$ is such a point :

$$M_j = M_0 + Y.x_j - X.y_j = 0 \; ; \quad .. \quad \text{(III, 13)}$$

introducing new co-ordinates x'', y'' with origin at $\mathcal{J}$ the displacement of the point $\mathcal{J}$ is obtained :—

$$\Delta x_j - \alpha.\Delta t.x_j = (1/EI)\,(Y.I_{x''y''} - X.I_{x''}) \quad .. \quad \text{(III, 14)}$$

also there is a similar equation for y_j.

IV. BENDING OF CURVED PORTIONS.

In practice pipe systems consist of straight portions connected by curved ones.

In a straight portion the stress is given by :

$$\frac{M r \sin \Theta}{I} \quad \text{(see Fig. 7)} \quad .. \quad \text{(IV, 1)}$$

which, for a given radius, has a maximum for $\Theta = \pm 90$ deg.

The moment of inertia is given by

$$I = \frac{\pi}{4}(r_e^4 - r_i^4) \quad .. \quad \text{(IV, 2)}$$

The stress diagram is a straight line (Fig. 7) and the neutral axis coincides with the axis of symmetry.

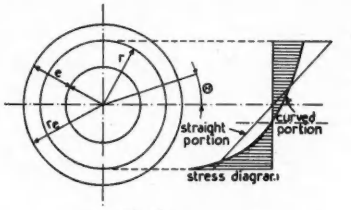

Fig. 7.

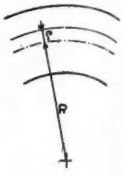

Fig. 8.

This is not so in curved portions ; the neutral axis is shifted towards the centre of curvature. If the stress formula for straight portions is applied, the stresses in the external fibres are over-estimated and those in the internal fibres under-estimated. In curved portions it is the fibre on the side of the centre of curvature which is most stressed.

For a radius of curvature R and a cross section S the tension at a distance ρ from the geometrical axis is (Fig. 8)

$$\frac{M}{RS} - \frac{\rho}{R+\rho} \cdot \frac{M}{K.R.S.} \quad .. \quad \text{(IV, 3)}$$

with

$$K = \frac{1}{4}\frac{r_i^2}{R^2}\left(\frac{r_e^2}{r_i^2} + 1\right) + \frac{1}{8}\frac{r_i^4}{R^4}\left(\frac{r_e^4}{r_i^4} + \frac{r_e^2}{r_i^2} + 1\right) + \frac{5}{64}\frac{r_i^6}{R^6}\left(\frac{r_e^6}{r_i^6} + \frac{r_e^4}{r_i^4} + \frac{r_e^2}{r_i^2} + 1\right) + \; .. \quad \text{(IV, 4)}$$

In practice, however, the formula for straight pipes is usually applied.

In curved portions the stresses affect the shape of the cross-section (see Fig. 9). Consider a portion with the angle ψ at the centre of curvature, a stress σ_t produced by the bending moment and the radial stress σ_r. If the

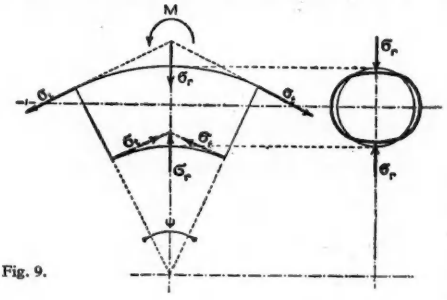

Fig. 9.

bending moment tends to increase the curvature, these stresses will produce a flattening of the cross-section. Von Kármán has shown that, for a given moment M, the stresses are thereby reduced and the flexibility increased.

This can be taken into account by multiplying the moment of inertia of the section by the "Kármán Number"[8]

$$Ka = \frac{1 + 12\lambda^2}{10 + 12\lambda^2} \quad \text{and} \quad \lambda = \frac{e\,R}{r_m^2} \qquad .. \quad \text{(IV, 5)}$$

(e thickness, R radius of curvature, $r_m = \frac{1}{2}(r_o + r_i)$).

This means that, everything else being equal, the factor k occurring in the above formulæ is just the reciprocal of the Kármán Number

V. STRESSES IN PIPE SYSTEMS.

Fig. 10.

It is sufficient to consider the principal stresses in the cross-section of a pipe. In fact, since the axis of the whole pipe system is in a plane, the only tangential stress that is not zero is the one due to the reaction component perpendicular to the curved pipe portion but it is usually negligible. The stresses are shown in Fig. 10.

1. *Axial Stress.* Axial stress results partly from internal pressure and partly from bending due to thermal expansion. (The weights of the pipes and fluid are neglected.) The first part is given by

$$\sigma_a' = \frac{p\,r_i^2}{r_o^2 - r_i^2} \qquad .. \quad \text{(V, 1)}$$

or if the thickness is negligible with respect to the radius

$$\sigma_a' = \frac{p\,r_i}{2\,(r_o - r_i)} \qquad .. \quad \text{(V, 2)}$$

The second part depends on the distance of the point considered from the neutral axis. For straight portions it is

$$M\,r \sin\Theta / I$$

for curved portions it is[7]

$$\frac{M\,r\sin\Theta}{I} \cdot \frac{1 - \dfrac{6}{5 + 6\lambda^2}\sin^2\Theta}{Ka} \qquad .. \quad \text{(V, 3)}$$

For a given λ and r the maximum stresses are at an angle Θ given by

$$\sin\Theta = \sqrt{\frac{5 + 6\lambda^2}{18}} \qquad .. \quad \text{(V, 4)}$$

But the $\sin\Theta$ thus obtained must be real, i.e. it must be

$$\lambda \leqslant 1{\cdot}472.$$

If this is the case the maximum stress is

$$\frac{Mr}{I\,Ka} \cdot \frac{2}{3}\sqrt{\frac{5 + 6\lambda^2}{18}} \qquad .. \quad \text{(V, 5)}$$

If $\lambda \geqslant 1{\cdot}472$ the maximum stress occurs when $\sin\Theta = 1$ and has the value

$$\frac{Mr}{I} \cdot \frac{12\lambda^2 - 2}{1 + 12\lambda^2} \qquad .. \quad \text{(V, 6)}$$

The distribution of the tension for different λ is represented in Fig. 11 taken from the book by Von Jürgenson[7].

These results can be summarized by

$$\sigma_a'' = \frac{Mr}{I} \cdot \beta \qquad .. \quad .. \quad \text{(V, 7)}$$

in which

$\beta = 1$ for straight pipes, $\beta = \dfrac{2}{3Ka}\sqrt{\dfrac{5 + 6\lambda^2}{18}}$ for curved portions, $\lambda \leqslant 1{\cdot}472$, and $\beta = \dfrac{12\lambda^2 - 2}{1 + 12\lambda^2}$ for curved portions, $\lambda > 1{\cdot}472$ .. .. (V, 8–10)

The stress due to the support reaction, or rather its component in the direction of the pipe, is often negligible.

The total axial stress is therefore

$$\sigma_a = \sigma_a' + \sigma_a'' \qquad .. \quad .. \quad \text{(V, 10)}$$

2. *Tangential Stress.* This results from the internal pressure and the bending moment. The internal pressure produces a stress

$$\sigma_t' = \frac{p r_i^2}{r_o^2 - r_i^2}\left(1 + \frac{r_o^2}{r^2}\right) \qquad .. \quad \text{(V, 11)}$$

for negligible thickness this is

$$\sigma_t' = \frac{p r_i}{r_o - r_i} \qquad .. \quad .. \quad \text{(V, 12)}$$

The stress due to bending vanishes for straight portions. For curved portions it is

$$\pm \frac{Mr}{I} \cdot \frac{18\lambda}{1 + 12\lambda^2}\cos 2\Theta \qquad .. \quad \text{(V, 13)}$$

The distribution of this stress in the outer fibre ($r = r_o$) and inner fibre ($r = r_i$) is shown in Fig. 12[7]. At the sections "O" the stress vanishes and the curvature is unchanged. The maximum stress is

$$\frac{Mr}{I} \cdot \frac{18}{1 + 12\lambda^2} \qquad .. \quad .. \quad \text{(V, 14)}$$

Hence

$$\sigma_t'' = \frac{Mr}{I}\gamma \qquad .. \quad .. \quad \text{(V, 15)}$$

when

$$\gamma = 0 \text{ for straight portions} \qquad .. \quad .. \quad \text{(V, 16)}$$

and $\gamma = \dfrac{18\lambda}{1 + 12\lambda^2}$ for curved portions (V, 17)

The total tangential stress is given by

$$\sigma_t = \sigma_t' + \sigma_t'' \qquad \text{(V, 18)}$$

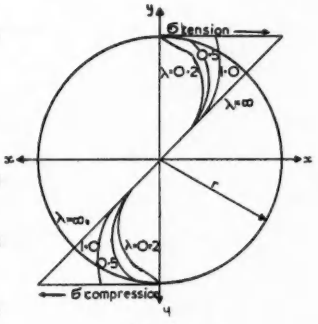

Fig. 11

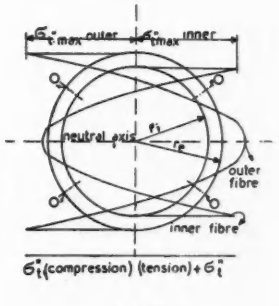

Fig. 12

3. *Radial Stress.* This stress depends only on the internal pressure and is given by

$$\sigma_r = p\left[\frac{r_i^2}{r_e^2 - r_i^2} - \frac{r_e^2 r_i^2}{r_e^2 - r_i^2}\cdot\frac{1}{r^2}\right] \quad .. \quad (V, 19)$$

it varies from $-p$ at the inside to 0 at the outside of the pipe.

In the case of plane pipe systems σ_a, σ_t and σ_r are the principal stresses. They vary from fibre to fibre. In practice the stresses on the inner and outer surfaces only are calculated. If σ_1, σ_2 and σ_3 are these three stresses in decreasing order of magnitude the appropriate theory of strength of the material used can be applied.

Safety Factor. Because of the accuracy of the above method a safety factor of 1·5 is usually sufficient. At 400 deg. C. (752 deg. F.) this coefficient is applied to the elastic limit, and above this temperature to the yield point of the metal.

BIBLIOGRAPHY.

1. CARLIER, H. *Etudes sur l'aptitude élastique des tuyauteries à vapeur au point de vue dilatation.* Ch. Delporte, Mons, 1920.
2. CARLIER H. *L'aptitude élastique des tuyauteries à vapeur au point de vue dilatation.* A. Carlier-Hermant, Brussels, 1925.
3. CARLIER, H. *Complement à l'étude sur l'aptitude élastique des tuyauteries à vapeur au point de vue dilatation.* A. Carlier-Hermant, Brussels, 1927.
4. CARLIER, H. *Aptitude élastique des tuyauteries à vapeur au point de vue dilatation.* H. Carlier, Waudrez-lez-Binche.
5. DE MARNEFFE, ALB. *Les constructions hyperstatiques.* 2nd edition. *Bibliothèque scientifique belge,* G. Thone, Liège, 1943.
6. S. TIMOSHENKO. *Strength of materials.* Van Nostrand Co., New York, 1934.
7. VON JÜRGENSONN, H. *Elastizität und Festigkeit im Rohrleitungsbau.* J. Springer, Berlin, 1940.
8. VON KÁRMÁN, TH. *Uber die Formänderung dünnwandiger Rohre, insbesondere Ausgleichsrohre.* Zeitschr. d. V.D.I., No. 45 1911.

SWITZERLAND

DETERMINATION OF THE PERMISSIBLE OXYGEN EXCESS IN THE OXY-ACETYLENE FLAME

By F. BÖHLER. (From *Zeitschrift für Schweisstechnik*, Vol. 36, Nos. 8 and 9, August and September, 1946, pp. 169-175, 191-195, 4 illustrations.)

UNTIL thirty years ago the aim of the welder was to make the ratio by volume (M) of O_2 and C_2H_2 in the oxy-acetylene flame equal to 1 (M = 1), to avoid the formation of FeO. It then became known that a raised value of M made higher working speeds possible, and that no harmful oxidizing effects resulted with ratios up to M = 1·4.

Part I deals with the equilibrium of the parts of the flame (CO, H_2, CO_2, H_2O) and the weld metal (Me). A neutral flame, neither oxidizing nor reducing, is one in which the pressures of the oxygen in the flame and of the oxygen in the weld metal are equal, so that there is chemical equilibrium between the terms Me, MeO O_2, CO, H_2, CO_2, and H_2O. Oxygen pressure in MeO depends solely on the temperature, but in the flame it depends on the temperature and the mixture ratio M. Oxidization takes place if the pressure of the oxygen in the flame predominates, and reduction if the pressure of the MeO prevails. The term MeO includes the oxides of alloying additions to the steel in rods.

M determines the oxygen pressure for any given temperature, and as each metal has a certain welding temperature, a certain value of M will be required to produce a neutral flame according to this percentage in each case.

Part II deals with the graphical determination of the mixing ratio (M) for neutral flames. A family of lines relate the oxygen pressure to a number of different temperatures, and when the log of the oxygen pressure is plotted against the reciprocal of the absolute temperatures the curves are straight for all values of M. These curves are nearly parallel for values of M more than 1·01.

Part III discusses the decomposition pressures of metal oxides. The partial pressure of the oxygen in the atmosphere amounts, of course, to 0·2 atmos. (abs.). For any particular metal oxide the decomposition pressure depends only upon the temperature. Below the temperature corresponding to 0·2 atmos. (abs.) oxidization will take place in air, and above it, reduction will occur. This applies equally to the welding flame where the partial pressure of the oxygen is only 10^{-1} to 10^{-20} atmos. (abs.) Oxides of silver, gold and platinum reach a decomposition pressure of 0·2 atmos. (abs.) below 300 deg. C., the common heavy metals reach only about 10^{-4} atmos. (abs.), and Manganese, Tungsten, Molybdenum, Chromium, Vanadium and Titanium drop to 10^{-20} atmos. (abs.). This drop continues through Aluminium and Magnesium, Boron and Silicon, to Carbon oxide which has a decomposition pressure at 1000 deg. C. of 10^{-60} atmos. (abs.). Plotting the log of the decomposition pressure against the reciprocal of the absolute temperatures a straight line curve is obtained for each metal oxide.

Part IV refers to the use of a graph of both the partial oxygen pressure of the flame and the decomposition pressure of the metal oxides plotted against the reciprocal of the absolute temperature. On the assumption that the welding temperature is about 100 deg. C. above the melting point this graph can be used to read off the limiting mixture ratio (M) of the flame which will avoid oxidization of any particular metal.

The author concludes that, with M exceeding 1, admixtures to the weld metal may be permitted to oxidize in order to form a protective coating to the weld, and the efficiency of such protection depends largely on the speed of welding. Oxidization of carbon cannot be avoided. The formation of oxide enclosures inside the weld need not, however, be very harmful unless the oxide is dissolved by the weld metal and on cooling leads to a spongy consistency. The following metals have oxides with a deleterious effect on welds in Iron, Cobalt and Nickel:—Iron, Cobalt, Nickel, Manganese, and to a smaller extent Chromium and Vanadium, whereas the oxides of Silicon, Aluminium, Boron, Calcium, Magnesium and Beryllium are relatively innocuous.

The use of rods in which the parent metal is alloyed with easily oxidized metals is based on the idea that the coating of oxides will protect the weld even if there is oxygen excess in the flame. Where great welding speed is important this excess is desirable because it leads to greater heat in the flame. If the parent metal is an alloy containing some relatively easily oxidized metals, the rod should, for ultimate homogeneity of the weld, contain double the percentage of these metals together with completely oxidizing additions

The reader is warned that the author's method does not apply to welding conditions which permit atmospheric oxygen to enter the flame.

HOGGING AND SAGGING TESTS ON ALL-WELDED TANKER "NEVERITA"

(From *Report No. R.1 of the Admiralty Ship Welding Committee.* H.M.S.O. London, 1946, 160 pages, 150 illustrations.)

EDITORIAL INTRODUCTION:

This book gives a comprehensive report on tests carried out on a scale and with a thoroughness hardly attempted before with a welded ship. This publication is the more remarkable as the tests were begun at a most critical time in Britain's history, just after the allied forces had launched their invasion of the European continent. It is not possible to reproduce more than a small proportion of the contents in these pages, but an attempt is also made of giving at least a few of the most instructive graphs, diagrams and photographs which are an essential feature of this outstanding document.

A great variety of strain measuring instruments were used in these tests and the comments on their efficiency should be of great value to those concerned with similar research in other fields.

Similar experiments have since been completed on a riveted tanker of the same form and general design. It is expected that the report will be published shortly, and it will then be possible, probably for the first time in the history of ship-building, to draw important comparisons between welded and riveted construction of ships scientifically tested under service conditions.

GENERAL.

THIS report describes a full-scale hogging and sagging experiment in still water on a welded 12,000-ton tanker, the methods used for determining the strains and deformations and the results obtained.

The experiment is one of a series planned by the Admiralty Ship Welding Committee, with the ultimate object of comparing the structural behaviour of similar riveted and welded vessels.

The main object of the experiment is to study the stresses set up on a cross-section of the ship, near amidships, by known changes in longitudinal bending moment, and to observe the deflection of the ship's girder under these changes.

In comparison with previous work of this kind, the committee was fortunate in this case in having the advantage of recent important developments in instrumentation and technique and a much more complete study was thus made possible. Many of the instruments and much of the technique was specially developed for this work. A full description of these developments has been included in these reports which it is hoped may benefit later research not only in connexion with ship structures but also in other fields of structural engineering.

The vessel was launched on February 26, 1944, its overall length is 485 ft. 5 in., the breadth 59 ft., the depth 34 ft., the displacement on designed draught 16,790 t. (salt water), the dead weight is 12,355 t. The class is Lloyds 100 A1, "carrying petroleum in bulk."

CONSTRUCTION.

It will be seen from the following figures that the vessel is divided by transverse and longitudinal bulkheads into 9 sets of 3 tanks. A deep longitudinal centre girder is fitted under the upper deck and a deep centre girder on the bottom. Horizontal scalloped gussets are fitted where the bottom longitudinals meet the transverse bulkheads. Details of these and other joints will be seen from the figures.

WELDING.

The entire structure is electrically arc welded, the exceptions being the connexions of the frames to the side shell plating and certain other details. The joints

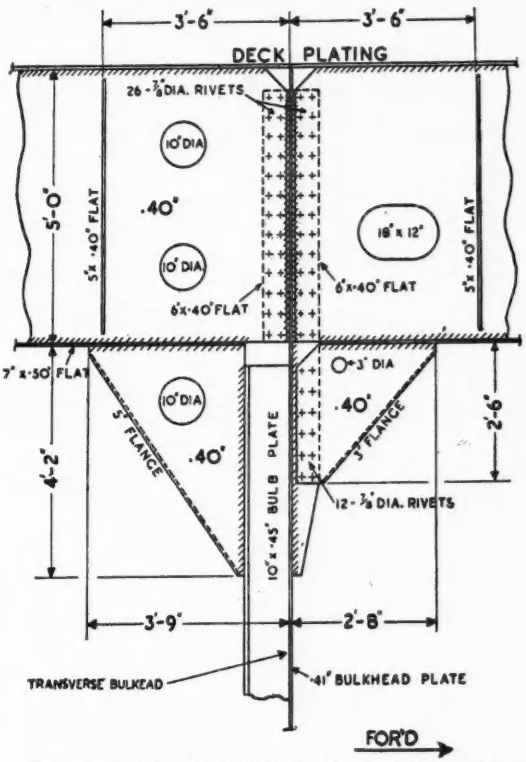

Fig. 1. **Connexion of deck centre girder to transverse bulkhead.**

between the longitudinal centre girder under the deck and the transverse bulkheads are riveted. This girder is continuous over the length of each tank, but it does not pass through the transverse bulkheads.

LOCAL CONDITIONS.

The experiment was carried out while the vessel was moored near Tyne Dock, County Durham, and was commenced immediately after the vessel was handed over by the builders. The recording of actual measurements was commenced on July 25 and was completed on August 8, 1944. The vessel was moored to buoys at bow and stern, heading up-stream, almost due east-west, and the wind and tide were never such that forces of any appreciable magnitude were imposed on the structure by the mooring cables.

OBJECTS OF THE EXPERIMENT.

In addition to the main object as described above there were further measurements to find the effects of local bending in one of the longitudinal bulkheads when subjected to water pressure on one side only. There was also an investigation into local bending of panels of bottom plating in different parts of the vessel. Deflections of transverse bulkheads were studied and stresses measured in various brackets and parts of the superstructure and observations were made of the stresses and deflections caused by irregular temperature distribution throughout the section of the ship.

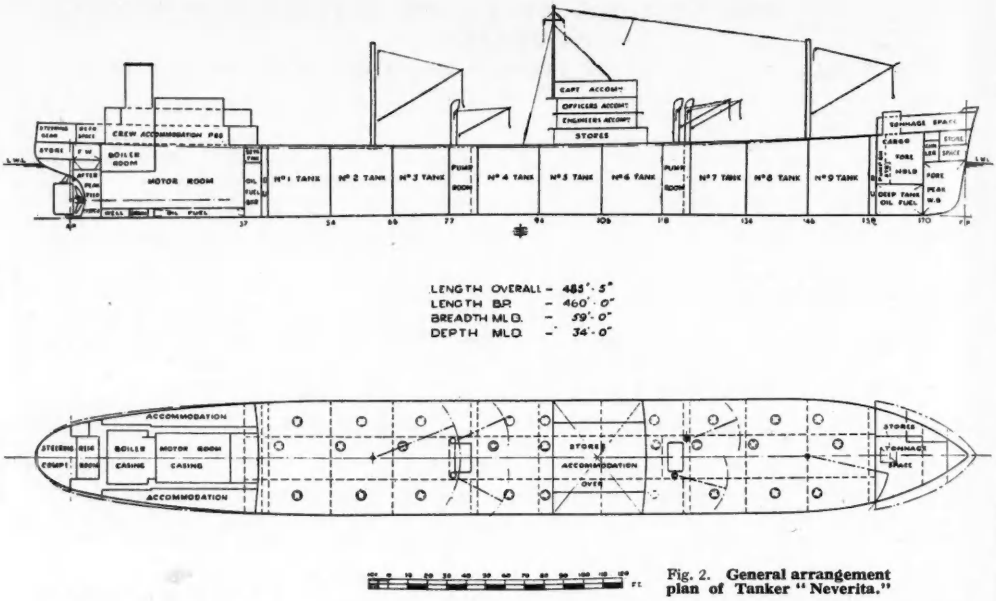

Fig. 2. **General arrangement plan of Tanker "Neverita."**

LOADING CYCLE.

The bending moments were induced by flooding different sets of tanks so as to produce fourteen different conditions of loading. Each of these conditions was designed to represent a specific case to give information on stress distribution, e.g. change of longitudinal bending moments, change of draught, and not less than 6 loading conditions were for the investigation of local stresses in the longitudinal bulkhead under hydrostatic pressure on one side.

In conducting the trials each condition was maintained for at least 8 hours and during that time the readings on all appropriate gauges were taken twice, once in the morning and again in the afternoon. This double reading provided a useful check against observational mistakes and gave a valuable indication of the fluctuations caused by changes in temperature distribution throughout the ship between the two sets of readings.

INSTRUMENTS USED.

A considerable amount of preliminary work was conducted in order to find gauges which were suited for the particular conditions existing during these trials. The requirements were for gauges giving accurate readings corresponding to about ¼ ton per sq. in. The instruments have to be easy to attach, they have to be quickly read and they must stand up to the unfavourable conditions of dirt and damp. Many existing gauges were found to fail in one or more of the essential features. It was, in general, necessary to develop gauges specially suited for the work. Due to wartime conditions it has not been possible in every case to secure all the refinements which would be desired. There are three classes of instruments used in these experiments :

(1) those for measurement of direct strain ;
(2) those to measure bending strain ;
(3) a group of instruments to find the deflection of the ship's girder.

The so-called direct strain gauges will usually record, in addition, any local bending strains, since it is only practicable to take measurements on outer fibres. One of the main purposes of the bending strain gauges is to identify these local bending strains in order that a true "middle of plate" strain can be obtained. These strains and stresses are important as it is only by knowledge of their values that an accurate comparison can be made between theory and practice, or between one ship and another. The bending strain gauges however were used for the value of their own readings when studying the bending of certain plated areas.

GAUGES FOR MEASUREMENT OF DIRECT STRAIN.

The choice of a suitable gauge length is one of the primary considerations. First, there is a very short base length of less than one inch of which the electric resistance strain gauge is an example. Gauges of this type record many minor concentrations of stress which may have no significance for the investigation of general stress distribution. Unless these gauges are used at very close centres an erratic stress picture may result. When making special study of local stress concentrations, gauges of these small base lengths are, however, desirable.

The second range of gauge lengths is one which forms a reasonable small percentage of the probable wave length of local bending stress ripples. This wave length is usually the spacing between frames or longitudinals and averages about 32 inches. A gauge length of about 5 inches will thus permit exploration of such stress variations with tolerable accuracy. Here a compromise has to be made between the desire to have the longest possible gauge length with the consequent high degree of accuracy, without, however, going much beyond the 5 inches so as not to have too high a percentage of the bending ripple wave length, as this would sacrifice accuracy.

The third range of gage length is much greater, such that many wave lengths of local fluctuations are included. It is possible, owing to the long base, to get a high degree of accuracy for strain even with a relatively inaccurate measurement of displacement between gauge points.

There are, however, several disadvantages attached to the use of such long gauge instruments. They ignore major stress concentrations which may be due to dis-

continuities forming only a proportion of the total gauge length. Practical considerations too are against using this long gauge length as it is difficult to find clear runs for the gauge without running foul of brackets and other fittings.

Inspection of the curves of stress on the cross-section (of which one or two out of many are included in this abstract) show that gauges of medium and long length give good agreement, apart from regions of discontinuity. There is reason to believe that this agreement extends to the short base gauges for the greater part of the section. Regarding the short base electric strain gauges, evidence is lacking in this report owing to technical difficulties with the zero readings of these gauges.

For the measurement of direct strain the following types of gauges were used :

(1) Tomlinson strain gauge, of 5 in. base length ;
(2) Maihak Acoustic gauge, 4¾ in. base length ;
(3) Long Base strain gauge, of 100 or 120 in. base length ;
(4) Fereday-Palmer strain gauge, of 21 in. base length ;
(5) Electric resistance strain gauge, of $\frac{13}{16}$ in. base length.

The matter of base length is also of importance were local bending strains are to be measured ; for practical reasons middle range lengths have been used between 3 and 6 in.

Direct measurements of deflection of members due to bending were also taken. For close detail work a row of dial gauges mounted on a rigid bar is used, but for large areas measurements are taken from stretched piano wires. Readings from this latter group of bending gauges are useful in giving a picture of the deflections caused, but it is almost impossible to convert the deflections into accurate stress values. The difficulty of conversion lies in the double differentiation involved. Although the experimental errors may be slight it is clear there will be large errors in any bending stresses so deduced. It is interesting, however, to compare these experimental deflections with the curves obtained by integrating bending strains and this operation can be conducted with considerable accuracy.

To measure local bending strains or bending deflections the following types of gauges were used :

(1) Ball type bending gauge, of 6 in. base length.
(2) Mushroom gauge, of 3 in. base length.
(3) Dial gauge bars.
(4) Deflection wires.

INSTRUMENTS FOR MEASURING DEFLECTION OF SHIP'S GIRDER.

Several completely independent means are available for this purpose. In these experiments three methods were used :

(1) Measurement of draught ;
(2) Water tube gauges ;
(3) Theodolite readings.

MISCELLANEOUS INSTRUMENTS.

A few additional instruments were used in these trials, e.g. Mercury thermometers and electric thermo-couples for measuring temperatures, and a float hydrometer to measure the specific gravity of the water.

For each of the instruments mentioned above the Admiralty report gives detailed descriptions, drawings and diagrams, instructions for fixing and reading, preparation of the gauge's position, data of the obtainable accuracy, the interpretation of readings, temperature effects, the theory of the various instruments and, perhaps most important of all, practical hints about experience gained and possible future improvements.

Just as an example the comments are here reproduced on the use of the *electric resistance strain gauge* for future trials.

This electric resistance strain gage consists of a fine filament of wire mounted on a paper backing. The gauge is stuck to the plating so that the strain from the latter is transmitted through the glue to the gauge. On straining the gauge the electrical resistance of the wire is increased partly due to the change in geometrical shape and partly due to an increase of resistance with increase of mechanical strain.

The results obtained were considered unreliable on account of zero drift caused by gradual change in the gauge resistance not associated with strain (the readings from these gauges were not used in the analysis). The comments given include the following points. On account of its short base length and overall dimensions this gauge fulfils a need that is not satisfactorily met by any mechanical instrument. It is highly desirable that a technique should be developed which would give satisfactory strain measurements over the fairly long periods of time involved in these trials. Investigations to improve the stability of the zero have been made both before and after the trials described herein, with the result that it is considered likely that a suitable technique will be achieved. The indications are that improvements in the technique could be effected by the following changes :

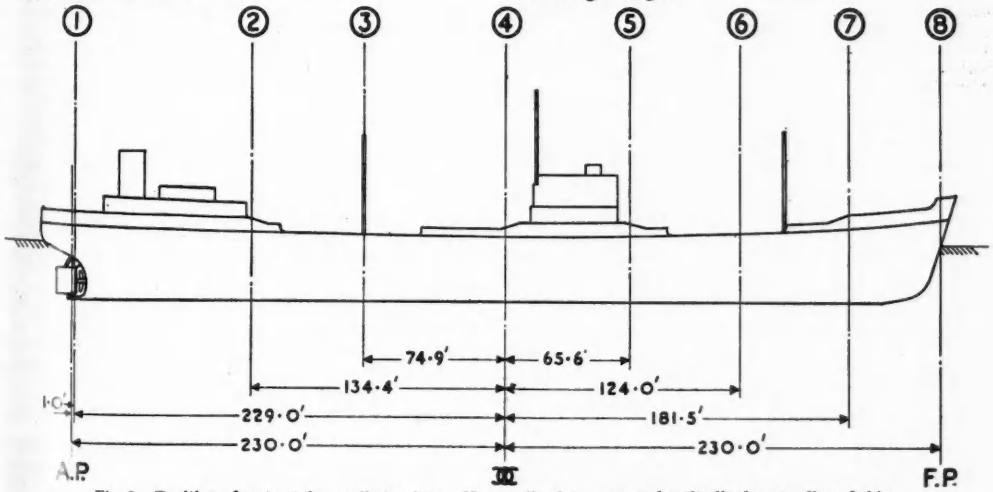

Fig. 3. Position of water tube reading points. Note : all points were on longitudinal centre line of ship.

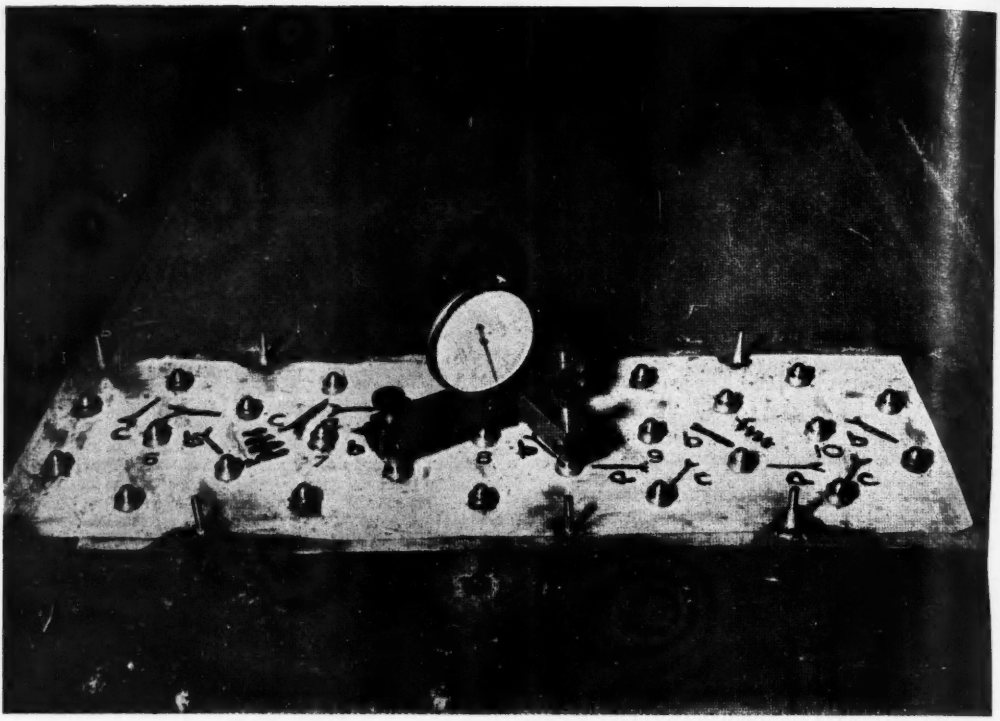

Fig. 4. **The ball type bending gauge.**

(*a*) superior protection of the gauge against moisture, including atmospheric moisture ;
(*b*) the electric current on individual gauges to be maintained only for sufficient time to take readings ;
(*c*) use of A.C. instead of D.C. on the bridge.

THE BALL TYPE BENDING GAUGES.

They can be seen in one or two of the following illustrations. These instruments are designed to measure bending strains on a 6 in. gauge length. The actual measurements are recorded by a dial gauge reading to 1/10,000 in. The gauge points consist of polished steel balls of ½ in. diameter, mounted in brass sockets which are fastened with adhesive to the plate surface. The original prototype gauge was made at the National Physical Laboratory by the late Dr. Tomlinson, and a number of subsequent gauges were built at the Engineering Laboratory of Cambridge University, under the guidance of Prof. J. F. Baker. The accuracy of these instruments is very good. The dial gauges can be read to 1/10,000 of an inch and by estimate to 1/100,000 of an inch. The good repetition usually obtained corresponds to a stress of ·074 t/sq.in. on a ½ in. plate. The adhesion of the ball sockets to the plating sometimes breaks down, specially on vertical surfaces, and the breakdown of one ball may affect the accuracy of as many as 9 adjacent readings.

The *deflection wires* mentioned above consist of lengths of 20 gauge steel wire stretched adjacent to bulkheads or side shell plating to provide base lines from which to measure deflections. They are used for measuring deflections over large panels of plating and in this respect differ from the other types of gauges which are designed to reveal local effects. They are also effectively used for approximate but rapid surveys of initial buckling in plated areas over which the theodolite can not be used. The readings are estimated to ·01 of an inch and results indicate that good repetition is obtained to approximately ·02 of an inch. The wires and measuring positions are easily and quickly rigged. One reading takes approximately 10 seconds but all the readings for one wire may take as much as three minutes depending upon the accessibility and spacing of the measuring positions.

The *water tube method* for measuring breakages records changes in deflections of the ship's girder as a whole. A series of open glass standpipes were placed at suitable points along the length of the ship, each standpipe being connected to a common main pipe running the full length of the ship. By means of graduated scales arranged beside the glass tubes the common water level could be read off, and the differences in reading reduced to changes in deflection.

Here the major source of error was the presence of air locks, but with the precautions taken, the general behaviour of the apparatus, and comparison with other methods for determining the deflection, the probable accuracy may be taken as being within ½ of an inch.

The *theodolite method* for observing breakages uses a theodolite capable of being read to one second of arc. The instrument is fixed in the wing of the navigation bridge and reading of the changes of vertical angles were taken on six targets spaced along the ship's length. With the precautions taken the readings were certainly accurate and repeatable to within 5 seconds of arc. Since the furthest target was 265 ft. from the instrument, the results can be taken as accurate to within about 1/20 of an inch.

FUTURE DEVELOPMENT OF INSTRUMENTS.

A summary of the characteristics of the types of instruments used is given in a special table, including also the immediate improvements proposed for the next

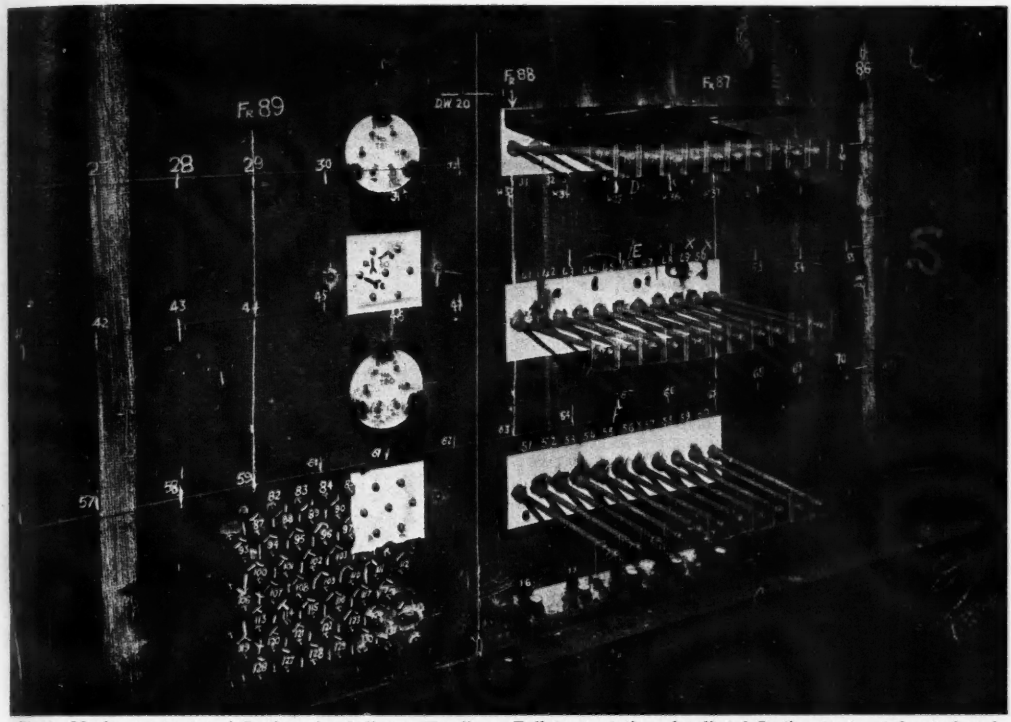

Fig. 5. **Mushroom gauges, deflection wire, ball area, Tomlinson Ball gauge stations, bending deflection gauge, at the starboard longitudinal bulkhead.**

trials of the series. An inspection of the properties of the various instruments reveals that the most suitable types are as follows, and these have been selected for long term use.

(*a*) Direct strain :
- (1) Acoustic gauges, with an additional set on elevated pads to eliminate local bending effects ;
- (2) Long base gauges, self-compensated for local bending ;
- (3) Electric resistance gauges, on both sides of plate around stress concentration points.

(*b*) Local bending strain :
- (1) Ball type gauge, used on areas only.

(*c*) Ship's deflection :
- (1) Theodolite method.

The Tomlinson gauge must be rejected on account of the time taken in reading. The Mushroom bending gauges are rejected similarly, as being redundant to the ball type gauge. Dial gauge bars and deflection wires are of doubtful use, as it is difficult to translate the results into terms of stress. The theodolite method for deflection is so accurate and simple as to supersede other methods.

REDUCTION OF OBSERVED READINGS TO STRAINS AND STRESSES.

For each type of instrument the method of reducing the instrument readings to strain is given in the appropriate section dealing with that instrument. In many cases the thickness of plating is involved in the reduction formulæ, and this has everywhere been taken as the thickness marked on the drawings, since it was usually impractical to measure the actual thickness.

In the reduction of strain to stresses the values of the elastic constants have been assumed to be :

Young's modulus E = 13,333 tons/sq.in.
Poisson's ratio $\mu = 1/3$

Where three directional strain gauge points are used the reduction to principal stresses and angle of orientation is done on a mechanical device based on the usual equations.

Then follows a chapter on calculation of the *theoretical bending moment and the deflection curves*, dealing with the calculated moment of inertia, the modulus of elasticity, the shearing deflection (based on the shear modulus of 5000 tons/sq.in. and a value of 1/3 for Poisson's ratio), and discussing the bending moments for standard wave conditions. For these calculations the ship was assumed to be in a fully loaded condition and in static equilibrium, firstly with crest of wave amidships, and secondly with the trough amidships.

It is conventional to take the wave length equal to the length of the ship between perpendiculars and to use a wave height from trough to crest of 1/20 of the wave length. Owing to the low freeboard of the ship in the fully loaded condition such a standard wave would have its crest amidships about 3 ft. above the top of the sheerstrake. In consequence of this effect, a somewhat shallower wave has been used of 1/30 of wave length, for both the hogging and sagging conditions. A further calculation has also been made using the conventional L/20 wave, assuming the freeboard to extend to the wave crest. It is interesting to compare the values calculated on these assumptions with the moments imposed during the trials.

BENDING MOMENTS IN TONS-FT., AT TEST CENTRE LINE FR. 88½

—	Hogging	Sagging	Range
Calculated values for L/30 wave	100,000	103,000	203,000
Calculated values for L/20 wave	144,000	157,000	301,000
Imposed values during trials	158,000	86,000	244,000

It will be noted that the range of moments between the experimental limits of hogging and sagging is about 80 per cent of the range of moments experienced under the two limiting conditions with a standard L/20 wave. It was not possible to extend the experimental range on account of the difficulty of imposing a large sagging moment in the still water trials.

The following chapters deal with the effects of the various loading conditions, the observations made, the measurements taken by means of an impressive array of instruments, and with the analysis of the tabulated results, in most cases shown in graphs and diagrams. The series of tests is headed by observations on the main hogging and sagging cycle, with the direct stresses produced on the main test section, and with the local bending stresses.

Then follows a discussion of the stresses caused by change of draught, then an investigation into the bending of a longitudinal bulkhead, and a rather detailed report on the exceptional local bending stresses found in the panel of the bottom plating in a port wing tank.

The behaviour of one panel of bottom plating is described next and the observations analysed in detail. Then follows a note on deflections in a transverse bulkhead, discussing the influence of bending of the transverse bulkhead on the bottom panel longitudinals.

The stresses in the strength deck forward were also looked into, and the stresses in the fashion plate at aft end of bridge, port side, are clearly illustrated.

A short note covers the stresses in bilge brackets and bracket of deep transverse frame to longitudinal bulkhead.

A more elaborate chapter deals with *stresses caused by temperature*, and this part is of special interest considering the arrangement of the test, the recording of temperature by modern instruments, and comparison of the observations with theoretical results.

Throughout a period of 12 hours a temperature cycle of readings was taken on a selection of gauges at half-hourly intervals without altering the loading. The records of the temperature taken with mercury thermometers and thermocouples at various parts of the ship during this 12-hour period were plotted in series of graphs giving the values as differences above sea temperature. The conditions prevailing during this investigation were as follows: At 9.30 a.m. when commencing the readings the sun was concealed by a morning mist which finally dispersed about noon. During this period the conditions were nearly static, with almost uniform temperature throughout the structure. Between noon and 2 p.m. the sun shone strongly with no cloud, and the deck temperature rose rapidly. The remainder of the steelwork followed this temperature rise by radiation and conduction, but at a much slower rate. About 2 p.m. a cooling breeze prevented any further rise of deck temperature which was then 90 deg. F., and for the next 3 hours the deck temperature fluctuated between 80 and 90 deg. F., as shadows of superstructure and fittings passed across the test section.

During this period the rest of the structure inside the tanks continued to warm up. Around 5 p.m. the sun became obscured in haze and the deck temperature began to drop at a steady rate. For some time the internal temperatures continued to rise, but then they too started to descend at a steady rate, more gradual than the rate of cooling on deck. By 9 p.m. the deck had cooled down but was still some 10 deg. F. warmer than the steelwork in the bottom.

The curves of principal stresses and deflections for the various gauges were plotted and showed a rise to as much as 3 tons/sq.in. The gauges were mostly on deck, which was exposed to direct solar radiation, and therefore passing shadows caused severe discontinuities in the values obtained.

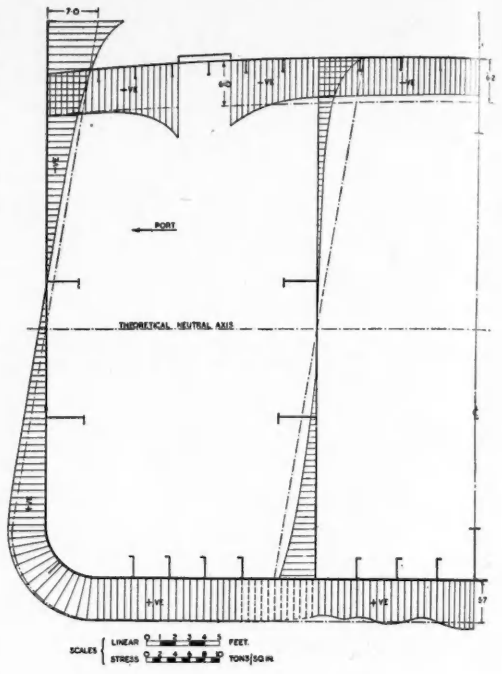

–VE DENOTES TENSILE STRESSES.
+VE DENOTES COMPRESSIVE STRESSES.

Fig. 6. **Main hogging and sagging cycle, distribution of longitudinal stresses over test section, stresses caused by change from neutral to hogging condition.**

On the centre keel girder which was of course permanently in shadow much smoother curves were obtained with the Fereday-Palmer gauges.

Regarding the electric resistance strain gauges it has been assumed that they were fully self-compensated for temperature, so that the readings obtained indicate true elastic strains.

A theoretical method for estimating the temperature stresses in a ship's structure was given in a paper to the Institution of Naval Architects.* This theoretical method has been applied to some of the experimental data obtained in the temperature cycle using the differences between the morning and afternoon temperatures. The theoretical stresses corresponding to the observed temperature differences have been calculated and plotted.

The basic assumption of this method is that the cross-sections of the vessel, remote from the ends, which were plane before bending remain plane after bending, regardless of whether the bending is caused by loading or by differential thermal expansions. From this assumption follows that the elongation of any elemental fibre due to the bending is proportional to the distance of the fibre from the neutral plane. If the temperature differences were also proportional to the distance from the neutral plane there would be curvature of the girder, but no stress. The linear temperature distribution required to produce the observed curvature without stress is termed the "virtual temperature distribution."

If, however, the virtual temperature distribution is

* O. Hurst Transactions of the Institution of Naval Architects, 1943, p. 74.

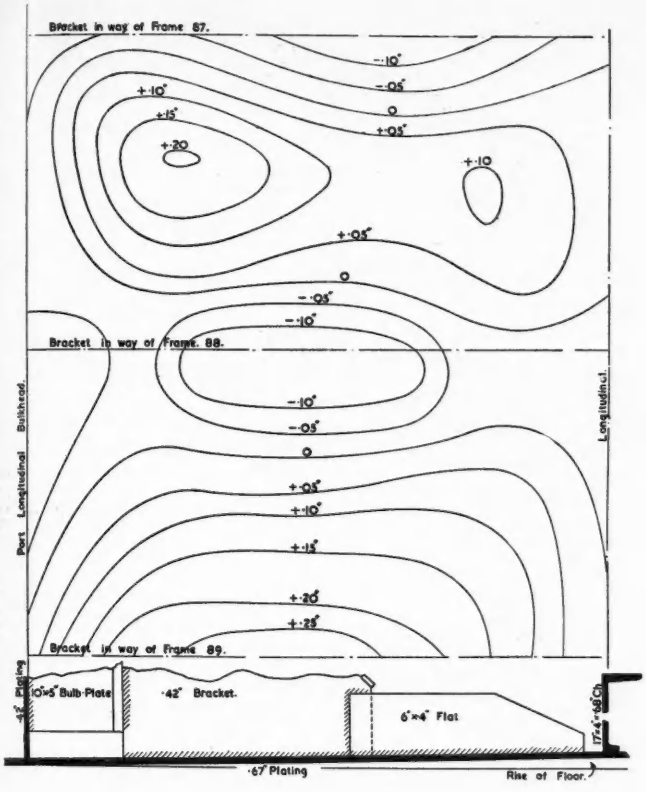

Fig. 7. **Bottom plating in port wing tank adjacent to longitudinal bulkhead. Surveyed levels of plating.**

not linear, stresses will be produced, and these stresses will be proportional to the departures of the actual from the virtual temperatures. Thus in any fibre the difference between the elongation due to the actual temperature distribution and the elongation required by the virtual temperature distribution will be due to elastic strain, from which strain the stresses of purely thermal origin can be deduced.

The deflection induced by the change in temperature can also be obtained from a constant b (which is constant for each cross section, but varies from section to section). The quantity b is a measure of the angular tilt of the cross-section to which it applies relatively to another cross-section at unit distance from it. This tilt is equal to the reciprocal of the radius of the curvature of the ship girder at the position of the cross section considered. Therefore the deflection will be

$$\delta = \iint \left(\frac{I}{R}\right) dx\ dx = \iint (b)\ dx\ dx$$

If the theoretical stresses are compared with the observed values, the following points will be noted.

Almost perfect agreement with the computed stress has been obtained with the Fereday-Palmer gauges Nos. 1 and 2. These gauges were sheltered from direct solar radiation, and since they were located on the centre line of the ship they were probably unaffected by lateral bending stresses due to one side of the ship being at a different temperature from the other.

The Tomlinson and Maihak gauges on the deck however show stresses greatly exceeding the theoretical values. This may be the result of local bending of the plating, which is indicated by the fact that the Maihak gauges on the underside of the plating often show tensile stress, while the Tomlinson gauges on the upper side show compression. In the cases where a Tomlinson gauge was directly over a Maihak gauge, the mean of the two gauges is in fair agreement with the computed values.

The long-gauge bases gave results which are in better agreement with the theory, probably due to the fact that these gauges are less affected by local bending.

In some cases high transverse stresses appear to have been set up and it is possible that the Poisson's ratio strains from these have modified the theoretical longitudinal stress distribution. For certain stations the transverse stresses were found to be of equal magnitude to the longitudinal stresses.

The computed hogging deflection of 1·88 inches is higher than the observed deflection of 1·28 inches. Amidships, however, the bridge structure shades the strength deck and it is unlikely that the section so shaded bends to any appreciable extent. The same applies to the forecastle and poop, but in those cases the influence on the overall deflection is smaller. These deductions, combined with other errors arising from the assumption of constant radius of curvature throughout the ship, may account for the discrepancy between the observed and computed values.

The theoretical method described seems in general to give results in fair agreement with experiments, but where sharp local temperature gradients exist, as for example where one part of the deck is in shade and another exposed to direct sunlight, there must be more complicated stress patterns due to temperature, which are not covered by the theory.

Fig. 8. **Long-base and Tomlinson gauge positions, upper deck and fashion plate, port side.**

PLATE SURVEYS TO MEASURE INITIAL BUCKLING OF PLATING.

Due to fabrication a certain amount of uneveness has to be expected in the plating. The survey was made around all plating on which strain gauges were attached. The deck and bottom were surveyed with theodolite used as a level, and all vertical plating was surveyed with string lines stretched over the four frame spaces. The survey was limited to finding the buckling along horizontal lines running fore and aft. Ideally the work should have been done with the ship in neutral longitudinal bending, so that no buckling would result from elastic strains. In practice it was found impracticable to do this, and most of the survey was made with the ship in loading condition No. 14, that is with a hogging moment of 100,000 ton ft.

For the deck and bottom plating it was found that the longitudinal stiffening effectively prevents any buckling in the longitudinal direction. For the longitudinal bulkheads and shell where the stiffening is vertical considerable buckling was shown. In places eccentricities equal to the plate thickness occurred here. It was not possible, however, to estimate with any certainty the buckling stresses by knowledge of the initial buckling in adjacent panels.

FINDINGS AND CONCLUSIONS.

A. BEHAVIOUR OF SHIP'S GIRDER.

(1) The measured changes in stress, after correction for local bending, are in fairly close agreement with the classical beam theory. Stress concentrations exist at structural discontinuities and there are a few unexplained variations.

(2) The stress distribution on the transversely stiffened side shell and longitudinal bulkheads shows less agreement with theory than that on the deck and bottom

(3) Transverse stresses of the order of 20 per cent of the longitudinal stresses have been observed. These show considerable unexplained fluctuations.

(4) The deflections observed in the ship's girder were slightly less than those computed on the assumptions adopted.

(5) The observations of strains and deflections in the ship's girder show no evidence of permanent set over the range of bending moments applied during the experiment.

B. LOCAL EFFECTS.

(6) High local bending stresses and deflections caused by changes in hogging and sagging moments were observed where the panels of plating had their lesser dimensions in the longitudinal direction. These high stresses and deflections are related to the initial deflections in the plating.

(7) High stresses and deflections due to hydrostatic pressure were observed in the lower part of the longitudinal bulkhead plating.

(8) Local bending stresses considerably in excess of the neutral fibre stresses due to hogging and sagging were observed.

(9) Local plastic yielding was observed in one panel of bottom shell plating.

(10) Where axial loading is imposed on plating having initial deflection due to unfairness or to hydrostatic pressure, the principle of superposition does not apply.

C. TEMPERATURE.

(11) Stresses of the order of 2 tons/sq.in. due to temperature variations of 30 deg. F. were observed in the deck plating.

THE STABILITY OF WATER DISTRIBUTION IN THE HEATING SURFACES OF FORCED FLOW BOILERS

By P. PROFOS. (From *Schweizer Archiv*, Vol. 13, No. 1, 1947, pp. 1-8, 11 illustrations.)

THIS article discusses the phenomenon that occurs under certain conditions of an uneven distribution of the water to parallel coil systems of forced flow boilers despite the fact that proper distribution would appear to be safeguarded by the action of the circulating pump. Irregularities in water distribution may lead to local overheating of the evaporating tubes, and consequently to boiler outage. A study of the problems involved has shown that two different phenomena exist which may occur either singly or together. In one case periodic fluctuations may occur in the rate of water flow passing through the individual tubes ; and in the other case an incipient irregularity in flow distribution will grow in magnitude without being accompanied by periodic fluctuations. Periodic disturbances in flow distribution may also occur in boilers of the natural circulation type, and the mechanism of this kind of disturbance is not yet fully explained. Disturbances of the second variety, that is, of the aperiodic type, can be analyzed with sufficient accuracy ; their appearance is generally bound up with systems of the type in which two manifolds are connected by parallel flow circuits consisting of tubes subjected to heating. It is a characteristic feature of this type of disturbance that it may occur even in cases where the parallel flow circuits are identical for interior tube diameter, length of circuit and shape of circuit, and are subject to identical heat inputs. In cases of this kind the origin of the disturbance is found to lie in the volume increase of the flow medium caused by the absorption of heat. In particular cases where the heat absorption causes the generation of steam it can happen that the pressure drop in one of the circuits increases with decreasing flow rate instead of decreasing, as would be expected. Or, vice versa, the pressure drop may decrease with a rising rate of flow. In this way the heat absorption of the flow medium will cause a weakening of the inherent resistance of the system to the occurrence of uneven flow distribution in the individual circuits. In fact, the heat absorption may become the cause of a permanent state of uneven flow distribution. In order to arrive at a criterion for the stability of the water flow distribution in a system, it is convenient to proceed from the consideration of the relationship that exists between the pressure drop and the throughput. This relationship can be determined by assuming the apportionment of equal amounts of fluid to the individual circuits. On the basis of constant pressure and constant heat absorption the relationship between the pressure drop Δp and the throughput G can then be computed for different admission temperatures of the flow medium. The functional relationship between Δp and G can then be graphically exemplified by the curves a, b, c, as shown in Fig. 1.

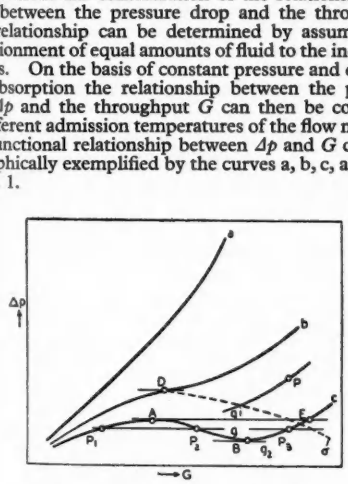

Fig. 1. **Variation of the pressure drop Δp with the throughput G for different admission temperatures and constant heat supply.**

Here a given operational condition is represented by a corresponding point P on a curve $\Delta p = f(G)$. The shape of these curves can serve as an indication of the degree to which the system tends to resist disturbances in flow distribution under a given operational condition. Resistance of the system against deviation from uniform flow distribution will prevail if the pressure drop Δp increases with the throughput G, that is to say, if $\frac{d\Delta p}{dG}$ has a positive value. Moreover, such a resistance will increase as $\frac{d\Delta p}{dG}$ increases, hence the steeper the curve $\Delta p = f(G)$ will be at the operational point considered. If the pressure drop curve droops, then even the smallest disturbance will tend to produce a state of uneven flow distribution ; and this tendency will be the more pronounced as the droop of the pressure drop curve becomes more pronounced. The stability of flow distribution obtaining under a given set of conditions will therefore be characterised by the differential quotient $\frac{d\Delta p}{dG}$ of the function $\Delta p = f(G)$.

Stable distribution will always obtain where the shape of the pressure drop curve is similar to that of curve (a) as given in Fig. 1. If the pressure drop curve resembles curve (b), then the system will be indifferent to flow distribution disturbances as far as the operational point D is concerned, because at this point it is $\frac{d\Delta p}{dG} = 0$. In cases where the pressure drop curve resembles curve (c), operational points with unstable flow distribution will exist. In order to be able to assess the conditions under which satisfactory operation can be maintained, knowledge of $\frac{d\Delta p}{dG}$ alone is not, however, sufficient ; and the following reasoning must also be applied.

Considering the section of the curve (c) confined by the horizontals g_1 and g_2, it is obvious that various flow distributions may obtain for one and the same pressure drop. Thus, for instance, flow conditions corresponding to $P_1 - P_2 - P_3$ can temporarily exist at one and the same time in various circuits of the system. Thus in some of the tubes the flow condition may be characterised by point P_1, while in other tubes the flow condition may correspond with the point P_2. A flow distribution of this kind, although stable in itself, is undesirable in view of the considerable and harmful inequality in flow through the tubes of the system. Stable and uniform flow distribution will therefore only obtain (a) if the differential quotient $\frac{d\Delta p}{dG}$ has a positive value, and (b) if only one flow rate G is coordinated with any one given pressure drop Δp.

This criterion rests upon the assumption of geometrically identical and identically heated parallel circuits which cannot of course be completely realised in practice. Moreover, certain other disturbing influences will be present. In order to obtain a flow distribution which meets practical requirements, that is to say, which is fairly insensitive to minor disturbance, a certain minimum value for the differential quotient $\frac{d\Delta p}{dG}$ will therefore be required. This quotient is not,

however, a suitable measure of comparative system stability, since its numerical value depends upon the set of conditions prevailing; and the dimensionless characteristic relationship

$$S = \frac{G \cdot d\Delta p}{\Delta p \cdot dG} \qquad .. \qquad .. \quad (1)$$

which expresses the variation in pressure drop as related to the variation in the flow rate would appear to be preferable. This characteristic relationship will be termed the *stability number*. According to its definition the stability number S expresses the variation per cent in the pressure drop if the flow rate is varied by one per cent.

The functionality of the pressure drop can be expressed by

$$\Delta p = K \cdot G^n \qquad .. \qquad .. \quad (2)$$

where Δp is the pressure drop, G is the flow rate, and K is the coefficient of flow resistance as applying at an arbitrarily chosen operational point P. By differentiating, it obtains

$$\frac{d\Delta p}{dG} = K \cdot n \cdot G^{n-1}$$

and it is therefore

$$n = \frac{d\Delta p}{dG} \cdot \frac{1}{K \cdot G^{n-1}} = \frac{d\Delta p}{dG} \cdot \frac{G}{\Delta p} = S$$

This shows the exponent n to be identical with the stability number as defined by equation (1), and it can therefore also be written

$$\Delta p = K \cdot G^S \qquad .. \qquad .. \quad (3)$$

This relationship provides a basis for the investigation of the stability of composite systems.

Another interesting relationship can be obtained by expressing the pressure drop by the equation

$$\Delta p = \frac{\lambda \cdot l}{d} \cdot \frac{\gamma}{2g} \cdot w^2 \qquad .. \qquad .. \quad (4)$$

where λ is the friction coefficient, $\gamma = 1/v$ is the specific gravity of the flow medium, g is the gravitational constant, w is the velocity of flow in the tube, d is the interior tube diameter, and l is the equivalent straight tube length of a flow circuit.

By taking into account the relationship

$$w = \frac{G \cdot v}{\pi/_4 \cdot d^2}$$

equation (4) can also be written

$$\Delta p = \frac{8 \cdot \lambda \cdot l}{\pi^2 \cdot g \cdot d^5} \cdot v \cdot G^2 \qquad .. \qquad .. \quad (4a)$$

In view of the fact that the specific gravity of the flow medium will vary over the tube length, a mean value v_m, for the specific volume must be introduced into equation (4a), this mean value being given by

$$v_m = \frac{1}{l} \int_0^l v \cdot dl$$

Formula (4a) will therefore take the form

$$\Delta p = \frac{8 \cdot \lambda \cdot l}{\pi^2 \cdot G \cdot d^5} \cdot v_m \cdot G^2 = K_1 \cdot v_m \cdot G^2 \quad (4b)$$

By introducing the value for Δp into formula (1) and differentiating, the following important relationship obtains,

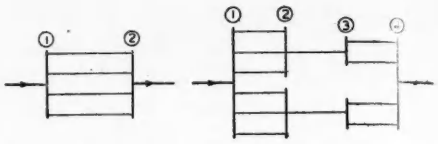

Fig. 2A. Simple circuit. **Fig. 2B. Composite circuit.** (Diagrammatic representation).

$$S = \frac{G \cdot d\Delta p}{\Delta p \cdot dG} = 2 + \frac{G \cdot dv_m}{v_m \cdot dG} \qquad .. \quad (5)$$

The relationships given above are applicable to simple systems (Fig. 2a), as well as to composite systems (Fig. 2b); but it should be noted that in the case of a composite system the stabilities of both the composite system as a whole (comprised between the headers (1) and (4) in Fig. 2b) and its component systems (comprised between the headers (1) and (2), and (3) and (4) respectively) must be examined. The equations (1) to (5) enable the numerical computation of the stability number to be carried out. Stability will obtain in a given case if the numerical value for S does not lie below a certain limiting positive value.

In the case of heated systems a maximum value of $S_{max} = 2$ — with the specific volume remaining constant — can obtain, as will be seen from equation (5) where in this case the term $\frac{dv_m}{dG}$ becomes zero. The choice of the magnitude of the stability number for a given case will depend upon the degree of agreement between the theoretically assumed operating conditions (particularly the assumption made with regard to the uniform heating of the individual circuits) and the conditions actually prevailing in a given case. Quite generally the influence of such adverse influences will be smaller the larger the value for S. This fact is exemplified by Fig. 3, which shows percentage deviation

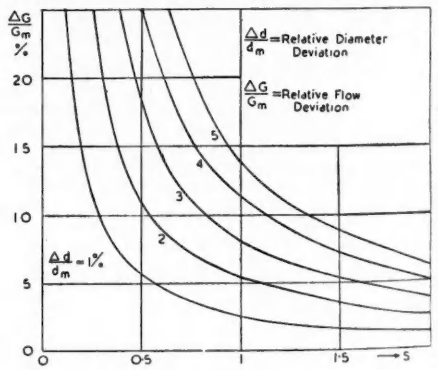

Fig. 3. Influence of tube diameter deviations upon flow rate for different S values.

of the flow rate from its mean value as a function of S for different deviations in the tube diameter of the individual circuits from the mean tube diameter. As will be seen from this graph, a tube 2 per cent smaller in diameter will pass 11·5 per cent less flow than the other tubes, the stability factor in this instance being $S = 0{\cdot}5$.

STABILITY UNDER PURELY EVAPORATIVE CONDITIONS.

Where the process of evaporation is exclusively concerned, computation of the stability of the system is based upon the fundamental equation (5). If the pressure drop in the system is not unduly large, the mean

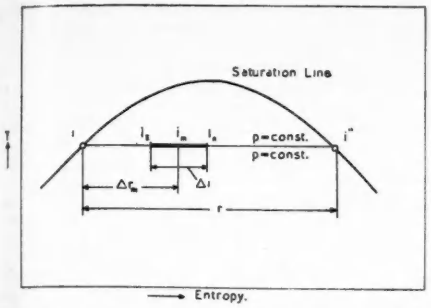

Fig. 4. **Explanatory diagram relating to the computation of the stability number in the case of evaporation alone.**

specific volume of the steam-water mixture can be expressed by

$$v_m = v' + \frac{v'' - v'}{r}\left(i_E - i' + \frac{\Delta i}{2}\right) \quad .. \quad (6)$$

where v' and v'' are the specific volumes of water and steam at saturation temperature, i is the heat content of the water in the condition of incipient evaporation corresponding with the mean pressure, and r is the latent heat of evaporation (Fig. 4). By introducing $\Delta i = Q/G$, the relationship between the mean volume and the flow rate G will then be expressed by

$$v_m = v' + \frac{v'' - v'}{r}\left(i_E - i' + \frac{Q}{2G}\right) \quad .. \quad (7)$$

By differentiating and rearranging it obtains

$$S = 2 - \frac{\Delta i}{2\left(r\dfrac{v'}{v'' - v'} + i_E - i' + \dfrac{\Delta i}{2}\right)} \quad (8)$$

We make

$$\Theta = r\frac{v'}{v'' - v'} \text{ and } \Delta r_m = i_E - i' + \frac{\Delta i}{2}$$

Here Θ is solely a function of the steam pressure and indicates the influence of the latter upon the stability. The factor Δr_m defines, as it were, the location of the preheating section in the evaporating zone ; as Δr_m is increased the stability number S will also increase.

In Fig. 5 the stability number is charted as a function of the final moisture percentage of the steam for various

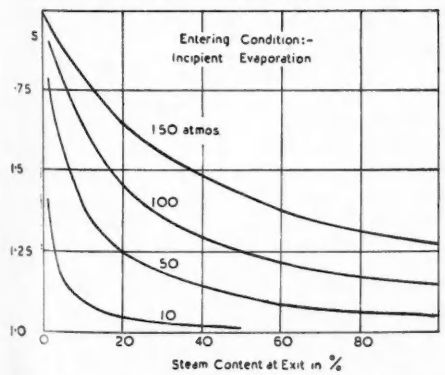

Fig. 5. **Stability of flow distribution in the case of evaporation alone. Functionality of S or function of steam pressure and steam content at exit of systems. Entering condition; Incipient evaporation.**

steam pressures, the initial moisture content being taken as 100 per cent. Referring to this graph, it will be seen that the stability factor decreases from its initial value of $S = 2$ to an increasing extent as the moisture content in the leaving steam is reduced.

STABILITY OF STEAMING ECONOMISER CIRCUIT.

In the case of a steaming economiser the mean specific volume of the steam-water mixture is found as

$$v_m = \frac{1}{2\Delta i}\left\{\Delta i^*(v' + v_E) + (\Delta i - \Delta i^*)\left[2v' + \frac{\Delta i - \Delta i^*}{r}(v'' - v')\right]\right\} \quad (9)$$

where $\Delta i^* = i' - i_E$ signifies the amount of preheating up to the point of incipient steam generation. By introducing $\Delta i = Q/G$ as before, v_m can be expressed as a function of the flow rate G, and by differentation the following expression for S is obtained from equation (5) :—

$$S = 2 - \frac{B \,.\, \Delta i^2 - A}{B \,.\, \Delta i^2 - C \,.\, \Delta i + A} \quad .. \quad (10)$$

where

$$A = \frac{\Delta i^*}{2}\left[(v'' - v')\frac{\Delta i^*}{r} - (v' - v_E)\right]$$

$$B = \frac{v'' - v'}{2r}$$

$$C = \Delta i \,.\, \frac{v'' - v'}{r} - v'$$

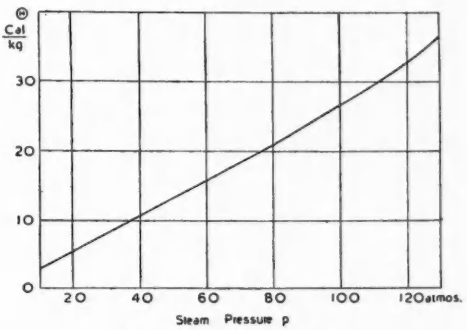

Fig. 6. **Variation of factor Θ with the pressure.**

For practical purposes the change in volume prior to incipient evaporation may be neglected, so that $v_1 \sim v'$ and equation (10) will thus take the simplified form

$$S = 2 - \frac{\Delta i^2 - \Delta i^{*2}}{\Delta i^2 + \Delta i^{*2} - 2\Delta i\left(\Delta i^* - r\dfrac{v'}{v'' - v'}\right)} \quad (11)$$

$\Theta = \dfrac{r \,.\, v'}{v'' - v'} = f(p)$ is plotted in Fig. 6 as a function of the pressure. This graph is typical of the influence exerted by the pressure upon system stability.

If complete evaporation is assumed, then for a given pressure the stability number S will be an exclusive function of the amount of preheating as expressed by Δi^*, that is, it will be

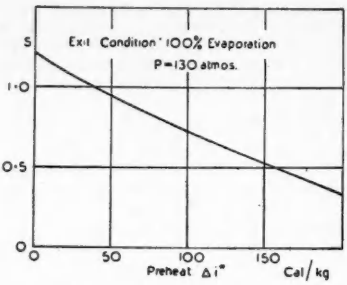

Fig. 7. **Stability in evaporating-economiser zone. Influence of preheating upon S in the case of complete evaporation.**

$$S = 2 - \frac{\Delta i^* + r/2}{\dfrac{\Theta}{\Delta i^* - \dfrac{}{r}} + r/2 + \Theta} \qquad .. \quad (12)$$

This relationship is charted in Fig. 7 for a pressure of 130 kg. per sq. cm. It should be noted that for $\Delta i^* = 0$ the expression for S becomes identical with that found for the case of purely evaporative conditions, that is, equations (8) and (10) become identical. The functional relationship between the stability number and the per cent steam content at the exit from the system for different degrees of preheating as expressed by equation (11) is graphically represented by Fig. 8, this graph being based upon a pressure of 130 kg. per sq. cm. Here the stability number is seen to decrease with the steam content up to a certain point, and then to rise again slowly. The loci of the minimum values for S are seen to lie on a curve shown in broken line in the graph.

Probably the most important conclusion to be drawn from equation (11) is that the greatest influence exerted upon the stability is due to the factor Δi^*, the value for S decreasing rapidly with rising values for Δi^*. This means that a long preheating section has an adverse influence upon the water distribution, and this is so in spite of the stabilising effect of the pressure drop in the preheating section. This deleterious effect of the preheating section can, however, be compensated for by increasing the water velocity, and with it the pressure drop in that section.

Fundamentally this measure is analogous to the well known employment of orifices at the inlet side of the heating surface.

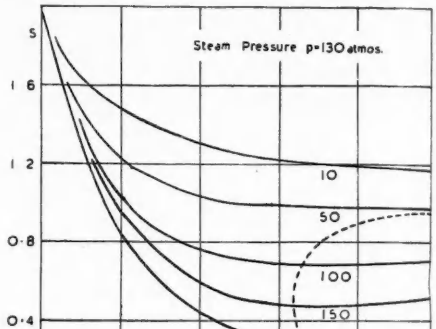

Fig. 8. **Stability in evaporating-economiser zone. Influence of preheating and steam content at exit upon the stability number S.**

CZECHOSLOVAKIA

SKODA UNIVERSAL LATHES

By Joseph Píč. (From *Strojnicky Obzor*, Vol. 26, No. 17-18, September, 1946, pp. 159-165, 10 illustrations.)

Greatly increased rates of metal removal, at higher cutting speeds, made possible by the use of carbide tools, has necessitated important changes in lathe design. New problems due to increased spindle speeds and power input have required the use of new bearings and lubricating systems, and greater strength, with rigidity, is essential to avoid troubles due to vibration. The brittle nature of hard carbide tool tips must be cared for by more robust design of the spindle, spindle-stock, tail-stock and lathe bed, and bearing surfaces must be amply disposed for continual service without developing backlash or side-play. Also the spindle must run freely in true dynamic balance to allow for machining accuracy and the results obtainable by fine finishing operations.

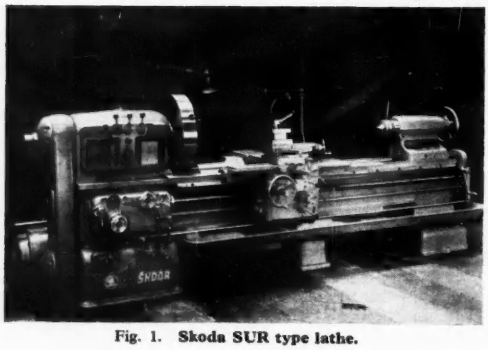

Fig. 1. **Skoda SUR type lathe.**

These features allow for the operation of machines to maximum capacity, but to obtain the full advantages offered it must be possible also to stop the rotation of the heaviest load on the face plate from high speeds very quickly so that changes of work can be made with a facility which reduces idle machine time. In this connection the value of multiple-speed motors can be realized if the automatic switch-off of the speeds is precise and reliable.

The Skoda S.U.R. Universal Lathes (see Fig. 1 and Table I) are soundly designed and constructed on these lines. In four types of medium size having centre heights from 260 to 400 mm., and ranges of spindle speeds from 1 to 130, which allow for slower work speeds when other

tool materials are used for screw-cutting, boring and reaming, etc., these machines give exceptional versatility. Spindles are driven by two-speed motors through twin multi-disk clutches, gears and silent chains, and these housed in the foot below the spindle-stock allow for the heat and vibrations generated at the clutch and brake to be damped out and not to be directly transmitted to the spindle. At low speeds the spindle is driven through the gears, and at high speeds directly by the chain. The spindle is provided with a surface-hardened flange to allow for the fixing of various clamping devices, and this is preferable to a threaded spindle end with which there would be a danger of loosening by the inertia forces due to accelerations and retardations of the work. It is supported in anti-friction bearings, whilst the power feed is on orthodox lines having settings for metric and inch pitches not affected by gear changing.

TABLE I. PRINCIPAL TECHNICAL DATA OF SKODA S.U.R. LATHES.

Type	Sur 260	Sur 300	Sur 350	Sur 400
Centre Height mm	260	300	350	400
Maximum turning dia. over bed, mm.	550	630	740	840
Maximum turning dia. over slide	300	380	470	570
Number of spindle speeds	32	32	32	32
Spindle speed range, r.p.m.	9·8-1250	8·5-1100	7·4-950	6·4-830

Longt. feed, number of steps	88
Longt. feed, range mm./1 turn of spindle	0·01-2·5
Transverse feed	0·45 × longitudinal feed
Threads :	
metric-pitch mm	0·2-120
Whitworth-threads/inch	1/4-120
Module mm. ..	0·125-30
Dia. pitch-Threads/1 in. dia.	17/8-64
Circular pitch, inch ..	1/128-3 1/4 in.
Motor power	6/16 kw = 8/22 H.P.
Motor r.p.m.	700/1350

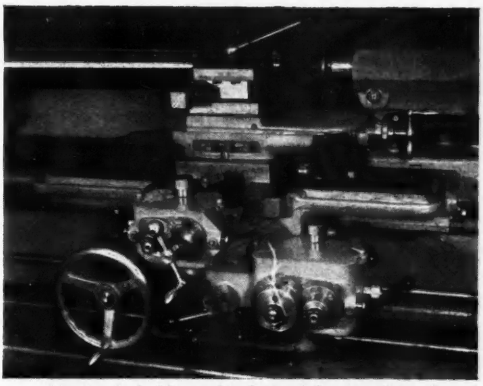

Fig. 2. **Switchboxes for determining lengths and diameters automatically.**

For switching off the power feed a device is incorporated in the slide which operates when contact is made with a stop on the lathe bed. This also serves as a safety device against overloads and is precise in actuation. Slide guides are comparatively long and related to the tool so that specific pressures between the sliding surfaces are low. All shafts run in ball-bearings, high-speed gears have case-hardened and ground teeth, gear-boxes are oil-tight and well lubricated, and the cast-steel face-plates are statically and dynamically balanced.

Without interference with the universal usefulness of these lathes they can be converted to high-output production machines by using special devices available for that purpose. The fitment of switchboxes to the longitudinal and transverse automatic feeds (Figs. 2 and 3)

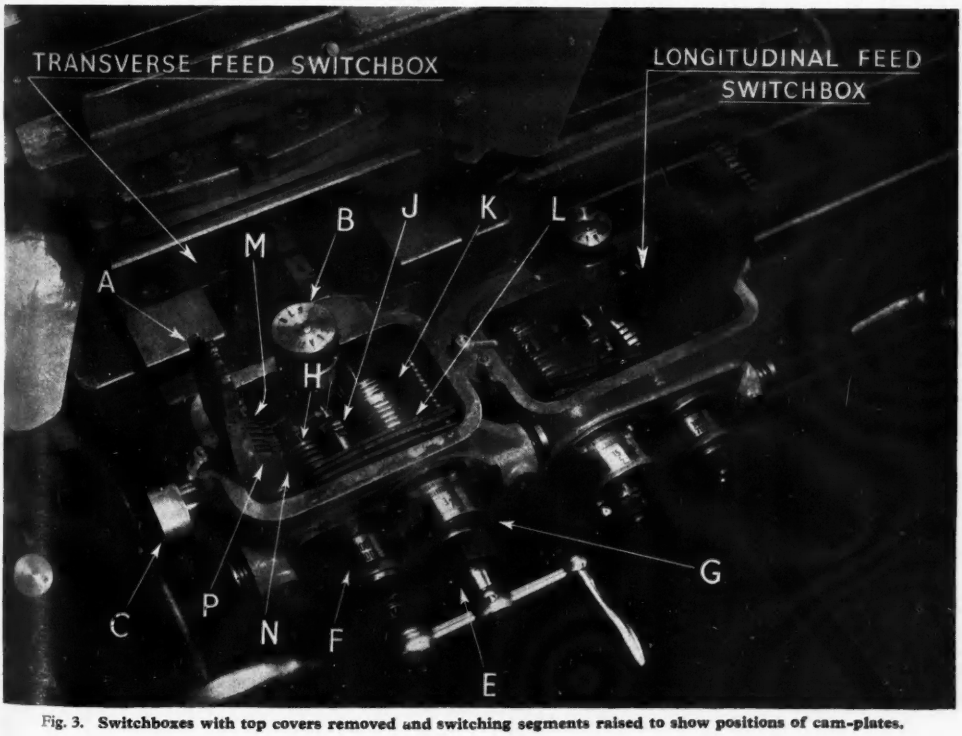

Fig. 3. **Switchboxes with top covers removed and switching segments raised to show positions of cam-plates.**

make it possible to turn stepped shafts to tolerances of ± 0·02 mm. on the lengths and ± 0·01 mm. on the diameters without measuring. The feed in the slide gear is automatically tripped after contact is made with fixed stops in the slide.

By turning a knob stops are selected and positioned, whilst adjustment is simplified by reference graduated drums which directly indicate the lengths and diameters desired for the work-pieces. The time taken in making these preliminary adjustments depends upon the number of stops used, and varies from 15 to 25 minutes, but the time saved is appreciable even when as small a number as three pieces are machined to the precision thus determined, and the method is undoubtedly economical.

For the transverse feed, the switchbox (see Fig. 3) is connected to the extended spindle on which a set of 12 cam-plates K, each having one tooth L, are mounted. The nut E locks the cam-plates in the positions they are set-up in. Mounted on a parallel shaft is a somewhat similar set of cam-plates H connected by gearing to the slide spindle, so that it rotates at a slower speed, and between the two shafts is a spindle J which, when knob B is rotated, is used to lower the segments A over the cams for the required switching operations.

On the shafts, drum indicators F and G are graduated for use in determining settings, and when the cam-plates are positioned and secured, by knob C and nut L, knob B is turned to lower the segments A. The centre parts P of the segments A rest upon the spindle J and the positions M and N rest upon the cams H and K respectively.

The operation for each individual pair of cam settings is that when the tool approaches the diameter desired cam H owers the segment and at the precise moment the tooth L on cam K contacts and pushes on the end of segment A. Segment A moves in response to this push and switches off the feed. The machine operator intervenes between each switching operation by turning the knob B for positioning the next segment.

The switchbox for the longitudinal feed operates in a similar manner and for turning stepped diameters it cuts off the traversing feeds when the required dimensions are obtained. When the cams in both boxes have been correctly set, and one diameter has been determined by the winding handle, and by measurement, the other diameters, and the lengths, are automatically obtainable by the switching operations. With sets of 12 cams, one, or any of that number, of diameters and lengths can be machined.

Small adjustments necessary when a worn tool is replaced are made by a special device not visible in Fig. 3, but these do not affect the cam-settings.

Examples of production times are given in Table II.

TABLE II. EXAMPLES OF TURNING ON S.U.R. 260 LATHE USING SWITCH-BOXES AND CARBIDE TOOLS.

			Time for 1 piece (min.)	
			With switchboxes	Without switchboxes
1	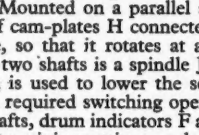	Material: Steel 50-60 kg./mm², 40 mm. dia.	3·5	15
2	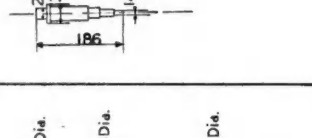	Material: Steel 70-80 kg./mm², 50 mm. dia.	10	50
3	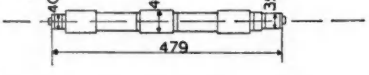	Material: Steel 70-80 kg./mm², 50 mm. dia.	7 (with air chuck and rapid slide movement 4 min.)	36
4	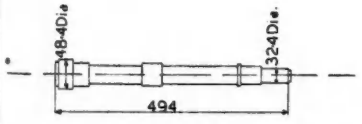	Material: Steel 70-80 kg./mm², 55 mm. dia.	7 (with air chuck and rapid slide movement 4 min.)	45
5	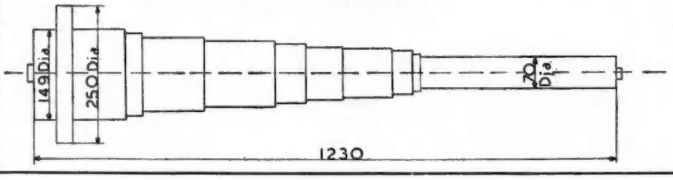	Material: Steel 70-80 kg./mm²., Forging. Weight of chips 95 kg.	56	165

THE PERFORMANCE RATIO OF THE BLOWPIPE FLAME WITH LEFTWARD AND RIGHTWARD WELDING

By F. BÖHLER. (From *Zeitschrift für Schweisstechnik*, Vol. 36, No. 12, December, 1946, pp. 246-253, 4 illustrations.)

In an editorial note it is stated that the superiority of the rightward welding method has so far been amply proved by practical welding tests. The author of this article produces confirmatory theoretical evidence from thermodynamic and physical considerations.

INTRODUCTION.

THE main difference between the old "leftward" and the modern "rightward" welding technique is illustrated by Figs. 1 and 2. Up to about 20 years ago the first was the only common practice in gas welding. With the blowpipe in his right hand, the filler rod in his left, the welder would proceed to the left. Since 1926, when C. F. Keel drew attention to the advantages obtained with righthand welding, this technique was gradually acknowledged as being superior and to-day, apart from special cases, rightward welding is generally practised. As shown in Fig. 2 the blowpipe precedes the filler rod, both moving to the right. The filler rod is thus kept between the flame and the molten puddle. With the older method the relative position of the blowpipe to the filler rod and the puddle is just reversed.

(The following may help to clarify the terminology : old method = leftward = "forward" technique new (Swiss) method = rightward = "backward" technique).

The advantages gained with the rightward method, especially the increased output, can be judged by comparing Figs. 1 and 2. With the older technique the axis of the blowpipe flame was more or less parallel to the surface of the molten puddle. With the rightward method, however, the gases from the blowpipe are directed at right angle against the molten metal, and their better heat effect is readily understood. Thus, the higher output with rightward welding is explained by the increase of heat transmission when changing the direction of the flow of the welding gases from parallel to perpendicular in relation to the surface of the molten metal. The conditions of this heat transmission, and their effect on the welding output, form the subject of the following notes.

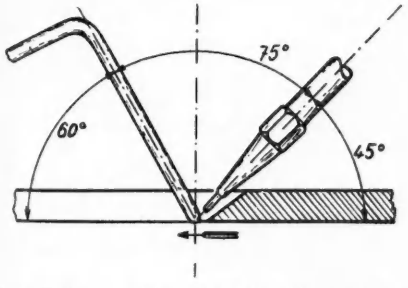

Fig. 1. **Leftward welding (this is the older technique).**

I. THE RATIO OF HEAT TRANSMISSION COEFFICIENTS WITH LEFTWARD AND RIGHTWARD WELDING.

In transmitting a quantity of heat Q, expressed in Cal. per hour, the following equation applies :

$$Q = \alpha F (t_G - t)$$

where α .. heat transmission coefficient in Cal. per m² per hour per 1 deg. C.,

F .. surface of the body in m²,

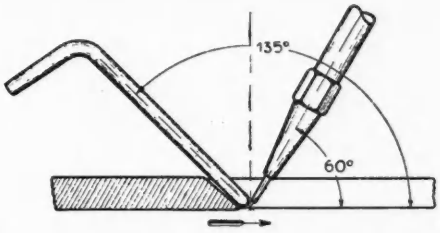

Fig. 2. **Rightward welding (this is the modern technique).**

t .. temperature of the body in deg. C.,

t_G .. temperature of the surrounding atmosphere in deg. C., where $t_G > t$.

This coefficient α represents the combination of all the factors which influence the heat transmission.

With $(t_G - t) = t_{\ddot{u}}$ representing the surplus temperature of the atmosphere compared with the temperature of the body, we have :

$$Q = \alpha F t_{\ddot{u}} \quad .. \quad .. \quad (1)$$

For processes of heat transmission which are comparable amongst themselves, e.g. the case described above and the case of the blowpipe gas directed at the surface of the molten metal, the following equation applies :

$$\alpha \cdot \frac{l}{\lambda} = C \cdot (Re)^n \quad .. \quad .. \quad (2)$$

Here l means a turbulence factor in metres,

λ the heat conductivity coefficient for the gas in Cal./m. per hour per deg. C.

C is a constant,

Re is the Reynolds number.

As a result of tests carried out by Reiher[1] in 1925 on water-carrying tubes of various cross sections exposed to a current of hot air at right angle to the tubes, the amount of heat transmitted from the air to the tubes was found to be represented by :

$$\alpha \cdot \frac{d}{\lambda} = C \cdot Re^{0.75} \quad .. \quad .. \quad (3)$$

where $d = \frac{U}{\pi}$

U .. circumference of the tube in m,

C .. a constant dependent on the cross-section of the tube.

For a circular tube d is its outer diameter.

Fig. 3 gives some of the results in graph form, with Reynolds numbers Re as the abscissa and $\alpha \cdot \frac{d}{\lambda}$ as ordinate, with loga ithmic scales. Equation (2) is represented by a straight line, its slope being determined by the power n. The series of straight lines refers to plane surfaces and tubes of various cross-sections, one or both sides exposed to the hot air current.

These test results are immediately applicable to the heat transmission from the blowpipe flame to the molten puddle, and a comparison can be made between the

1. Forschungsarbeiten für Wärmeforschung, Heft 269, 1925 published by Marhold, Halle.

performance of leftward and rightward welding. The lines I and VI can be taken to represent the heat transmission from the blowpipe flame to a perpendicular or parallel plane metal surface, providing the length of this surface is limited to about 50 times the flame diameter, and this applies in welding practice.

In welding practice, however, the surface of the molten metal is never quite plane, and the direction of the welding gases will not quite agree with the test assumptions. Taking all the circumstances into account, the lines II and V in Fig. 3 may safely be assumed to represent conditions during welding, the first with the flame directed at right angle, the second with the flame parallel to the surface of the molten puddle. The ratio of the two heat transmission coefficients will be

$$\frac{\alpha_N}{\alpha_P} = \text{constant} = 4{\cdot}0 \quad .. \quad .. \quad (4)$$

where α_N .. coefficient of heat transmission with right angle flame,

α_P .. coefficient of heat transmission with parallel flame.

II. THE RATIO OF WELDING OUTPUT WITH LEFTWARD AND RIGHTWARD WELDING.

The above ratio, however, can not directly be applied to a comparison between the welding output figures obtained with the two welding techniques. In practice the angle between blowpipe and molten metal surface varies all the time during welding, and even the average angle will largely depend on the welder's skill and experience. The author, when observing an experienced welder, found the following average values of this angle :

10 deg. with leftward welding,
75 deg. with rightward welding.

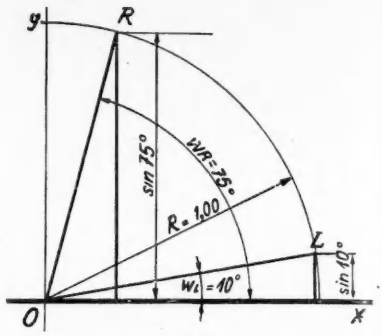

Fig. 4. **Relative position of blowpipe axis to surface of molten metal with leftward and rightward welding.**

Assuming the quantities of transmitted heat are proportional to the sine of the angles, the ratio is obtained from :

$$\frac{\alpha_R}{\alpha_L} = \frac{1 + 3 \sin 75 \text{ deg.}}{1 + 3 \sin 10 \text{ deg.}} = \frac{3{\cdot}9}{1{\cdot}53} = 2{\cdot}55 \; .. \; (5)$$

where the indices *R* and *L* refer to " right " and " left."

Fig. 4 illustrates the relative position of these angles :

OX .. surface of the molten puddle,
OL .. relative direction of the blowpipe flame with leftward welding,
OR .. relative direction of the blowpipe flame with rightward welding,
OY .. the ordinate axis, at right angle to metal surface OX.

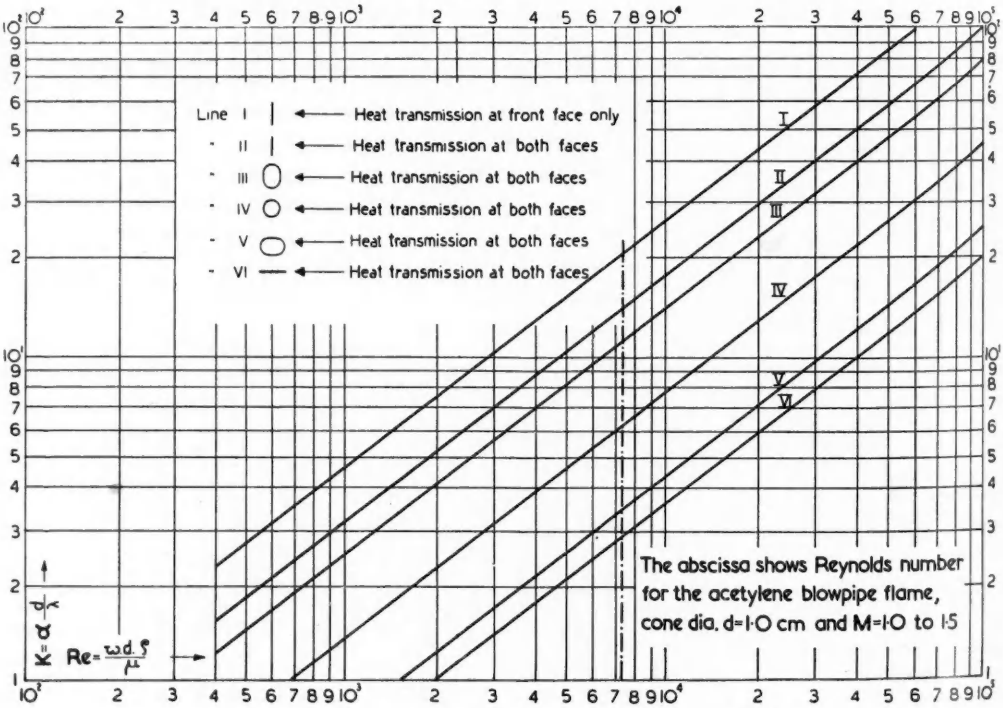
Line I — Heat transmission at front face only
II — Heat transmission at both faces
III — Heat transmission at both faces
IV — Heat transmission at both faces
V — Heat transmission at both faces
VI — Heat transmission at both faces
I
II
III
IV
V
VI
The abscissa shows Reynolds number for the acetylene blowpipe flame, cone dia. d=1·0 cm and M=1·0 to 1·5
Re=ωd.ρ/μ

Fig. 3. **Heat transmission from hot air current to tubes and plates placed at right angles.**

From equation (5) and Fig. 4 the ratio $\frac{\alpha_R}{\alpha_L}$ can readily be determined for different sets of angles of inclination. The surface of the molten puddle is, however, not smooth and plane, but uneven and rough, and this is another contributory factor in reducing the differences in performance of leftward and rightward welding.

Giving due consideration to all these influences, the ratio as obtained by a well experienced welder will be as follows :

$$\frac{\alpha_R}{\alpha_L} = \frac{3{\cdot}75}{1{\cdot}60} = 2{\cdot}34 \quad .. \quad .. \quad (6)$$

The same ratio will apply to the quantities of heat actually transmitted by welding, and therefore also to the welding output obtained by leftward and rightward welding, and is valid for any size of nozzle and Reynolds number.

The ratio of welding times is the reciprocal value, i.e. :

$$\frac{\alpha_L}{\alpha_R} = \frac{1{\cdot}60}{3{\cdot}75} = 0{\cdot}43 \quad .. \quad .. \quad (7)$$

which means, in practical terms, that rightward welding of a given job takes only 43 per cent in time, labour and gases, as compared with leftward welding. With less experienced welders an average ratio of 50 per cent will apply, other conditions being equal.

RUSSIA

CRITICAL SPEEDS OF ULTRA-CENTRIFUGALS

By V. I. Sokolov. (From *Journal of Technical Physics*, Vol. 16, No. 4, 1946, pp. 463-468, 2 illustrations.)

In the chemical industry difficulties are sometimes encountered because of unstable operation of ultra-centrifugals, resulting in a number of cases in breakdowns and undue wear of working parts. In cases of this kind it has not always been possible to find an explanation for the phenomena involved, and it is for this reason that the author has set himself the task of clarifying the phenomena bound up with the passage of an ultra-centrifugal through its critical speed.

The rotation of a solid body can be expressed by Euler's equations, which in the form proposed by Nicola can be written as follows :

$$\frac{d\sigma_1}{dt} + q_1\sigma_z - r_1\sigma_k = L_1, \quad \frac{d\sigma_k}{dt} + r_1\sigma_1 - p_1\sigma_z = L_k,$$

$$\frac{d\sigma_z}{dt} + p_1\sigma_k - q_1\sigma_1 = L_z \quad .. \quad .. \quad (1)$$

In Fig. 1 the axis of symmetry z of the rotor of the centrifugal is seen to pass through the point of origin O_1, of the three axes ζ, η, and ϑ of a system of coordinates. The nodal line I is a perpendicular upon plane ϑz and line k is a perpendicular upon the axes z and I. The rotation of the rotor of the centrifugal can be considered as representing the regular precession of a symmetrical gyroscope without movement of its own. The angular speed ω of the rotor, therefore, is the speed and ϑ the axis of this precession.

Neglecting the angular speed of the rotor, or more strictly, assuming the system I, k, z at rest with respect to the axis ϑ, we have

$$p_1 = \dot{\beta} \; ; \; q_1 = \omega \sin\beta \; ; \; r_1 = |\, \omega + \dot{\alpha} \,| \cos\beta \quad (2)$$

The speed $\dot{\alpha}$ is the result of the Coriolis force and is small as compared with ω. In order to simplify matters, we assume that

$$r_1 = \omega \cdot \cos\beta \quad .. \quad .. \quad (2a)$$

or, in other words, we assume that the principal axis z of the rotor always remains in the plane including the vertical (i.e. original disposition of the rotor axis) and that it revolves at the constant angular speed ω. The centre of inertia of the rotor will be assumed to lie along the axis of symmetry O_1, O_2. The moments σ_1, σ_k, and σ_z will then be given by

$$\sigma_1 = Ap \; ; \; \sigma_k = Aq \; ; \; \sigma_z = Cr,$$

where A and C are equatorial moments of inertia (with respect to point O_1) and polar moments of inertia respectively.

In consideration of formula (2) we then have

$$\sigma_1 = A\dot{\beta} \; ; \; \sigma_k = A\,\omega \sin\beta \; ; \; \sigma_z = C\,\omega\cos\beta \quad .. \quad (3)$$

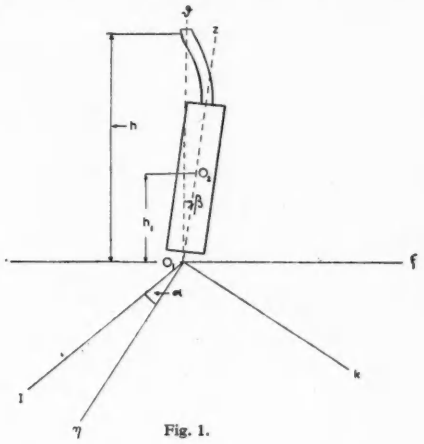

Fig. 1.

In linear representation it is

$$p_1 = \beta \; ; \; \sigma_1 = A\dot{\beta} \; ; \; q_1 = \omega\beta \; ; \; \sigma_k = A\,\omega\beta \; ;$$
$$r_1 = \omega \; ; \; \sigma_z = C \cdot \omega \quad .. \quad .. \quad (4)$$

By making $L_k = L_z = 0$ (equations (1)), the moment of the external force imparted to the rotor with respect to axis I will be given by

$$L_1 = -\delta_{11} h^2 \sin\beta + Gh_1 \sin\beta, \quad .. \quad (5)$$

where δ_{11} is the force causing a single revolution of the rotor spindle ; G is the weight of the rotor, and h and h_1 are the distances indicated in Fig. 1. By neglecting G and approximating $\sin\beta = \beta$ we obtain

$$L_1 = -\delta_{11} h^2 \beta \quad .. \quad .. \quad .. \quad (6)$$

The Euler equations will thus take the form

$$\omega^2 \,|\, C - A \,|\, \beta = -\delta_{11} h^2 \beta \quad .. \quad (7)$$

As the uneven distribution of the mass of the rotor will cause a deviation from the vertical by the angle β_0, equation (7) can also be written

$$\omega^2 \,|\, C - A \,|\, \beta + \beta_0 \,| = -\delta_{11} h^2 \beta \quad .. \quad (8)$$

Hence

$$\beta = \beta_0 \frac{\omega^2}{\frac{-\delta_{11} h^2}{C - A} - \omega^2} \quad .. \quad .. \quad (9)$$

and the critical speed is therefore found as

$$\omega_{crit} = \sqrt{\frac{\delta_{11}\, h^2}{A - C}} \qquad \ldots \qquad \ldots (10)$$

In the type of ultra-centrifugal normally employed the rotor is of conical shape. In order to determine δ_{11}, the spindle may be considered as a cantilever beam as shown in Fig. 2. For this shape the author finds

$$\frac{1}{\delta_{11}} = \Delta_{11} = \frac{4l^3}{\pi E \mid R - r_0 \mid^3}\left[\frac{r_0}{R^2} + \frac{1}{3r_0} - \frac{1}{R} - \frac{r_0^2}{3R^3}\right] \quad (11)$$

and the critical speed as

$$\omega_{crit} = \sqrt{\frac{h^2 \pi E \mid R - r_0 \mid^3}{\mid A - C \mid \left[\frac{r_0}{R^2} + \frac{1}{3r_0} - \frac{1}{R} - \frac{r_0^2}{3R^3}\right] 4l^3}} \quad (12)$$

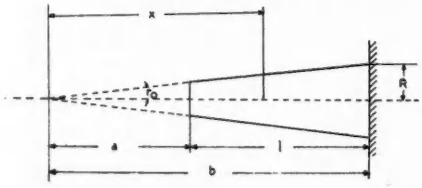

Fig. 2.

As ultra-centrifugals are operated at speeds higher than the critical, the problem of the passage of the rotor through the critical speed range cannot be neglected. There are two forms of passage through the critical speed range. In the first of these, the critical speed range is traversed at high speed which excludes an inadmissible growth of forced oscillation energy. This may be said to apply to small centrifugals. The second form of passage is accompanied by a limitation of the deflection of the spindle when passing the critical speed, this limitation being effected by the restraining action of the rings. This is the most frequent form, and it will be investigated here on the basis of the method suggested by Kapitza.

As Kapitza has shown, the critical point divides two qualitatively different rotations. In the first type of rotation the gyroscopic moment produced by the stabilizing forces of the spindle is given by the left hand side of equation (8). At a certain angular speed ω_1 the head of the rotor will touch the restraining surfaces. If e denotes the clearance between the head and the ring, then the angle of inclination of the rotor will be $\beta_1 = \frac{e}{h_3}$ where h_3 is the distance between the lower supporting point and the restraining ring. By introducing this value for β_1 into equation (8) and solving the latter for ω_1^2 we obtain

$$\omega_1 = \omega_{crit}\frac{e}{h_3\,\beta_0 + e} \qquad \ldots \qquad \ldots (13)$$

where $$\omega^2_{crit} = -\frac{h^2 \cdot \delta_{11}}{C - A}$$

When the speed of the rotor has reached the value ω_1, the deflection of the spindle ceases to increase owing to the action of the restraining ring. Upon contacting with rising angular speed, the head of the rotor is pressed by the centrifugal force against the restraining surface. But when the friction force prevailing between the head and the ring has reached a certain magnitude, the rotor begins to slide along the ring in opposite direction and the spindle instantly straightens. The speed ω_2 corresponding to the straightening can be computed as follows. The contacting of the rotor with the restraining ring will diminish the magnitude of the moment produced by the external force as given by equations (1). To the moment of the elastic bending force is added the moment of the reaction forces Qh_3 of the ring.

If γ represents the angle between the plane in which the gyroscopic moment acts and the plane of the deflection (comprising the point of contact) then the moment exerted at the point of contact will be given as

$$\omega_2 \mid C - A \mid \mid \beta_1 + \beta_0 \cos\gamma \mid \qquad \ldots (14)$$

and with Q representing the reaction force of the ring, it becomes

$$\omega^2 \mid C - A \mid \mid \beta_1 + \beta_0 \cos\gamma \mid = -\delta_{11} h^2 \beta - Qh_3 \quad (15)$$

The slipping of the rotor head on the surface of the restraining ring is accompanied by the appearance of a tangential force μQ, where μ is the friction coefficient. The existence of a motion of the first order will then be conditional upon

$$\frac{\beta_0\, \omega^2 \mid A - C \mid \sin\gamma}{h_3} > Q\mu \qquad \ldots (16)$$

With the use of Kapitza's method we find from equations (15) and (16) that

$$\frac{1}{\mu}\sin\gamma - \cos\gamma > \frac{\beta_1}{\beta_0}\frac{\omega_2^2 - \omega_{crit}}{\omega_2^2} \qquad \ldots (17)$$

$$\frac{\omega_2^2}{\omega^2_{crit}} = \frac{\beta_1}{\beta_1 - \beta_0\sqrt{1 + \frac{1}{\mu_2}}} \qquad \ldots (17a)$$

where ω_2 is the angular speed corresponding to straightening of the spindle. The condition for the passage through the critical speed can be given in the form

$$\frac{\beta_1}{\beta_0} > \sqrt{1 + \frac{1}{\mu^2}} \qquad \ldots \qquad \ldots (18)$$

and with e denoting the clearance between rotor head and ring, it finally obtains

$$\frac{e}{h_3\,\beta_0} > \sqrt{1 + \frac{1}{\mu^2}} \qquad \ldots (19)$$

The inequation (19) shows that the rotor of the centrifugal cannot pass through the critical speed if the clearance between the head and the ring is small or if the unbalance of the rotor is large. The increase in the size of the clearance is, however, limited by considerations of spindle strength.

If σ_z is the maximum permissible spindle stress, the maximum permissible clearance will be given by

$$e = \frac{l^2\,\sigma_z}{E \mid R - r_0 \mid^3}\left| r_0 R^2 + \frac{R^4}{3r_0} - R^3 - \frac{r_0^2 R}{3}\right| \quad (20)$$

where R is the greatest radius of the spindle, and r_0 is its smallest radius. The maximum pressure acting upon the upper bearing during passage of the spindle through the critical speed may be found as

$$x_1 = \frac{\omega^2_{crit} \mid A - C \mid \beta_0}{h^3} \qquad \ldots (21)$$

The author points out that the analysis given above should be of considerable value to factories producing ultra-centrifugals as it clarifies the influence exerted by the rotor clearance, the friction coefficient, and the unbalance of the rotor upon the passage of the rotor through the critical speed.